Production of exotic nuclides in nucleus-nucleus collisions in the Fermi-energy domain

M. Veselsky

Institute of Physics, Slovak Academy of Sciences,
Dubravska cesta 9, Bratislava, Slovakia
e-mail: fyzimarv@savba.sk

and

G.A. Souliotis

Physical Chemistry Laboratory, Department of Physical Chemistry, University of Athens, Athens, Greece,
and
Cyclotron Institute, Texas A&M University,
College Station, USA,

Abstract

The available experimental data from nucleus-nucleus collisions at beam energies from the Coulomb barrier up to 70 AMeV and various projectile-target asymmetries are investigated. The scenario involving pre-equilibrium emission in the early stage followed by deep-inelastic transfer or incomplete fusion leads to consistent agreement in most of the cases. The participant-spectator scenario starts to play role at energies around 50 AMeV for very asymmetric projectile-target combinations in inverse kinematics. At beam energies around and above

50 AMeV there are signals of the mechanism of neutron loss (dynamical emission) preceding the thermal equilibration of the massive projectile-like fragment. At beam energies below 10 AMeV, deep-inelastic transfer appears to be the dominant reaction mechanism, with contribution from the possible extended evolution of nuclear profile in the window (neck) region, mostly in the case of heavy target nuclei.

The achieved level of understanding of the reaction mechanism provides a suitable starting point to consider production of secondary beams in the Fermi energy domain. The comparison with other reaction domains, such as spallation and fragmentation, suggests that this option can be competitive for production of very neutron-rich nuclei around the N=50 and N=82 shell closures. Observation of isoscaling, namely the exponential scaling of product yields with initial isospin of the projectile-target system, can in principle be used for prediction of production rates in the reactions of exotic secondary beams.

Production of secondary beams in the Fermi energy domain requires specific technical solutions, including ion-optical devices with angular acceptance up to 10 degrees, such as superconducting solenoids, and effective event-by-event tagging procedure for an in-flight scenario or a highly effective gass cell for production of high-purity secondary beams. A comparative advantage is offered by the possibility that the primary beam can be easily eliminated, since the majority of exotic products is emitted at angles away from zero degrees.

Introduction

During almost century of nuclear physics studies, only approximately one half was investigated of up to 6000 nuclei stable against nucleon emission. The region of β-stable nuclei, which occur in the nature, covers only small fraction of nuclei between the lines of proton and neutron stability (driplines), where the binding energy of proton or neutron reaches zero. Nuclei away from the region of β-stability are not abundant in the nature and in order to investigate them it is necessary to prepare them in laboratory through nuclear reactions. Known β-unstable nuclei consist mostly of proton-rich nuclei, produced in compound nucleus and spallation reactions. Properties of proton-rich nuclei were investigated to the proton dripline from the light nuclei up to the proton-rich fissile nuclei, where decreasing fission barrier

becomes the limiting factor for production. The situation differs on the neutron-rich side. Only few regions are known, most thoroughly the light nuclei up to the oxygen, produced via fragmentation of heavier nuclei, where the neutron dripline was already reached. Heavier neutron-rich nuclei are known mostly in the region of light and heavy fission fragments. An extensive area of very neutron-rich nuclei still remains to be investigated.

The main difficulty in production of neutron-rich nuclei is that, due to absence of the Coulomb barrier, emission of neutrons is the most effective way od de-excitation. Intense emission of neutrons from the highly excited (hot) nuclei explains the relatively easy production of proton-rich nuclei. In order to produce neutron-rich nuclei, the excitation energy acquired during the nuclear reaction must be low enough and the neutron-rich nuclei should be produced primarily in the so-called cold processes with minimal neutron loss due to emission.

Out of the presently used production mechanisms of the neutron-rich nuclei, reactions of protons with the heavy fissile nucleus such as uranium appear most advantageous, both in direct or inverse kinematics. Direct kinematics is routinely used at ISOLDE facility, where the high energy proton beam hits the uranium carbide target. The ISOL technique is used to transport exotic nuclei into the ion source, followed by charge breeding and transport to detection system. While the ISOL technique allows high intensity of the primary beam, limitations arise from the complex extraction technique, which can be specific for a given product, and from the loss during transport and ionization. Inverse kinematics is used at the GSI facility in Darmstadt, where the uranium beam hits a hydrogen target and the secondary products are separated using the separator FRS. The advantages of such technique are flexibility, relatively easy identification of secondary products and relatively simple transport to detection system or secondary target. The limiting factor is the intensity of the primary beams. The dominant mode of the production of neutron-rich nuclei is the symmetric fission of uranium-like nuclei, excited during primary interaction with protons of the target. Even if such a method allows to produce wide range of neutron-rich nuclei, there still remain large regions of neutron-rich nuclei which are not accesible by this method.

Use of fragmentation reactions is limited by the fact that projectile nucleons are stripped by the target and the production cross sections are independent of the target neutron-to-proton (N/Z) ratio. Neutron excess is reached by stripping the maximum possible number of protons and lesser number of neutrons. To reach even higher neutron excess it appears necessary to cap-

ture additional neutrons from the target. Such effect is in principle possible in the reactions of nucleon exchange, which dominate at beam energies around the Fermi energy (20 - 50 AMeV). Highly precise experimental data are rather scarce at present, mostly due to the charge distributions of reaction products, leading to a complex procedure of identification and separation.

Analysis of available experimental data

In this section we will present a systematic analysis of available experimental data on production of projectile-like residues in the nucleus-nucleus collisions at beam energies ranging from the Coulomb barrier to about 70 AMeV.

Four projectile energy domains are defined :

- low energies up to 10 AMeV - domain where complete fusion is a common reaction channel, and also transfer reactions are observed
- transitional energies from 10 AMeV to 20 AMeV - domain where low energy reaction channels gradually evolve into picture typical for the Fermi energy domain. Also the domain where pre-equilibrium emission starts to contribute.
- energies around the Fermi energy (from 20 to 50 AMeV) - proper Fermi energy domain where binary dissipative collisions such as nucleon exchange and incomplete fusion are main reaction channels, but where already the mechanisms typical for higher beam energies may contribute.
- fragmentation energies above 50 AMeV - domain where fragmentation mechanism appears as increasingly dominant, however binary dissipative collision still can play role

Apart from beam energy, the reaction scenario is determined by the ratio between projectile and target masses (collision kinematics). Three scenarios are identified:

- normal kinematics - target is heavier than projectile, for mid-heavy beams typically consisting of heavy material such as gold, lead or fissile material such as thorium or uranium
- (nearly) symmetric collisions - projectile and target mass are comparable
- inverse kinematics - projectile is heavier than target

The goal of this analysis is to systematically explore majority of the combinations of the beam energy and kinematics by using available experimental data corresponding to individual combinations and to observe evolution of contributing reaction mechanisms. First we will describe the relevant reaction mechanisms, then we will discuss implementation and interplay of various model calculations in the simulations of experimental data and the model analysis of individual reactions will follow. Initially we will explore the nearly symmetric nucleus-nucleus collision in the proper Fermi energy domain and the analysis will then extend into neighboring regions.

Reaction mechanisms around the Fermi energy

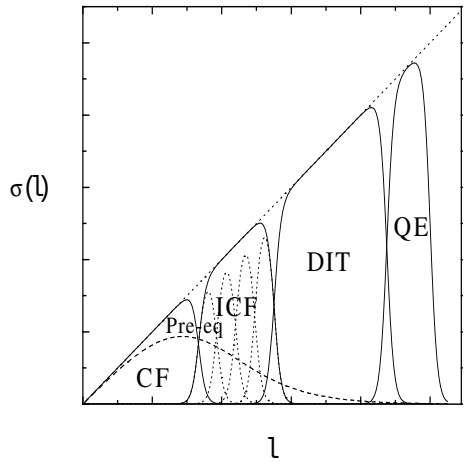

Figure 1: Development of the reaction mechanisms in nucleus-nucleus collisions in the Fermi energy domain. Cross section contributions are plotted schematically as a function of initial angular momentum.

A large variety of reaction mechanisms has been observed in nucleus-nucleus collisions in the Fermi energy domain (20 - 50 AMeV) depending on the impact parameter, projectile-target asymmetry and the projectile energy. The reaction mechanisms typically observed are [1]:

- peripheral elastic and quasi-elastic (QE) scattering/transfer reactions around the grazing impact parameter.

- deep inelastic transfer (DIT) reactions at semi-peripheral impact parameters with partial overlap of the projectile and target and a significant part of the relative kinetic energy transferred into internal degrees of freedom of the projectile and target.

- incomplete fusion (ICF) reactions at central impact parameters with a typical participant-spectator scenario. At energies around the Fermi energy the participant zone typically fuses with one of the spectator zones (typically heavier) thus creating a highly excited composite nucleus. At most central impact parameters the complete fusion (CF) can occur.

- pre-equilibrium emission of direct particles, caused by onset of two-body nucleon-nucleon collisions at central and mid-peripheral impact parameters. Pre-equilibrium emission precedes the ICF/CF and DIT reactions.

While such a scheme is well established, there are still many open questions related to the development of isospin-asymmetry in nucleus-nucleus collisions in the Fermi energy domain. Studies of isospin degrees of freedom in the nucleus-nucleus collisions in the Fermi energy domain reveal many interesting details of the reaction scenario. Recently, an enhancement in the production of neutron-rich nuclei was observed in peripheral nucleus-nucleus collisions [2, 3], which can be related to the effect of neutron-rich surface of the target on the nucleon exchange. Recent experimental observations in the semi-central collisions signal that the neutron-rich mean-field can play role in the re-separation phase, leading to fast transfer of neutrons in this phase [4] or to dynamical emission [5]. Large uncertainty exists e.g. in the transition from the regime of binary collision (DIT or ICF) to the high-energy participant-spectator scenario.

Methods of model calculations

The model calculations in the nucleus-nucleus collisions at beam energies below 100 AMeV can be performed in various ways, significantly differing among themselves. There exist various mathematically sophisticated concepts modelling the evolution of the nuclear mean field while other methods consider evolution of nucleonic cascade. Due to large variety of phenomenological reaction mechanisms, identified in the experiments, it appears justified to define the domains (in terms of beam energy and impact parameter) where specific reaction mechanism dominates and determine the evolution of each individual collision based on initial beam energy and impact parameter,

as described above and implemented e.g. in [1]. Following paragraphs will provide list of most important reaction mechanism and describe their typical implementations.

Deep-inelastic transfer (Nucleon exchange)

In the Fermi-energy domain, peripheral nucleus-nucleus collisions can be described theoretically using the model of deep-inelastic transfer, in combination with an appropriate model of de-excitation. Deep-inelastic transfer (DIT) occurs when interaction of the projectile and target leads to formation of di-nuclear configuration which exists long enough to allow intense exchange of nucleons through the "window" formed by interaction of mean-fields in the neck region. Transfer of nucleons leads to gradual dissipation of the kinetic energy of relative motion into internal degrees of freedom such as excitation and angular momentum. After re-separation the hot projectile- and target-like prefragments with approximately equal sharing of excitation energy are formed and undergo de-excitation via subsequent particle emission or multifragmentation. Very good description of experimental data from the peripheral collisions in the Fermi energy domain was obtained [6] using the Monte Carlo implementation of the DIT model of Tassan-Got [7], when combined with appropriate de-excitation code like SMM [8] or GEMINI [9]. SMM represents the statistical model of multifragmentation (SMM) and GEMINI implements the model of sequential binary decay (SBD).

Incomplete fusion

In the semi-central and central collisions in the Fermi energy domain one can assume that di-nuclear configuration is not formed and the participant-spectator scenario (as described in detail below) becomes probable. However, the participant zone will not necessarily evolve independently but can be captured by either the projectile- or the target-spectator zone. The relative probabilities of capture by the projectile or the target spectator zone can be determined by comparing the respective numbers of neighboring nucleons in both spectator zones. In the symmetric collisions the capture by either of the spectators is equally probable while for asymmetric systems the capture by heavier spectator dominates. The capturing spectator and participant zone form a hot fragment while the remaining spectator zone is much colder. The excitation energy of the hot fragment is obtained by energy balance of

incomplete fusion while for the cold fragment it is determined assuming that the part of the kinetic energy of relative motion between the cold fragment and participant zone is transferred into heat via collisions of the spectator and participant nucleons along the separation plane. The kinetic energy and the direction of the cold fragment is determined randomly using the double differential cross section formula based on the Serber approximation [10].

Participant-spectator scenario

At the sufficiently high projectile energy the incomplete fusion (fusion of participant and one of the spectator zones) will not be possible and the cold or relativistic fragmentation regime will be dominant. Several geometrical models of fragmentation have been proposed before where projectile and target are supposed to follow a straight trajectory determined by an impact parameter [11]. Other works assume a classical Coulomb trajectory up to the closest approach configuration and only later nuclei are supposed to follow straight line [12, 13]. In the work [1], a classical Coulomb trajectory of the intermediate projectile-target system was assume without making any additional assumptions. A minimum distance between the intermediate projectile and target is used as a principal parameter of the geometric overlap scenario. The volume of the participant zone is determined randomly from the interval with limiting values given by the abrasion-ablation formula and two-sphere overlap formula. As a result, one participant and one or two spectator zones are created in the fragmentation stage. Their masses are determined proportionally to the determined volumes and the charges of the spectators are determined according to the combinatorial probability density [14].

Pre-equilibrium emission

The pre-equilibrium emission (PE) is a process where fast particles are emitted prior to the equilibration of the system at projectile energies above 10 AMeV. For reactions induced by heavy ion beams a model of nucleon exchange, similar to the model of deep-inelastic transfer but assuming propagation of transferred nucleon through the accepting nucleus, was developed [15]. In the present work, we use a phenomenological description [1] based on similar assumptions as the exciton model. The probability of pre-equilibrium emission for a given reaction stage is evaluated using the formula

$$P_{pre}(n/n_{eq}) = 1 - e^{-\frac{(n/n_{eq}-1)^2}{2\sigma^2}} \quad (1)$$

for $n \leq n_{eq}$ and equals zero for $n > n_{eq}$, where n is the number of excitons at a given stage and n_{eq} is the the number of excitons in the fully equilibrated compound system (consisting of both projectile and target) for a given excitation energy.

Statistical models of de-excitation of hot nuclei

A main assumption of the statistical models describing various processes is that a certain stage of the process can be identified where the available phase-space determines final probability distribution of the possible exit channels. For instance, in statistical description of the fully equilibrated compound nucleus, the probabilities of various evaporation channels are determined by available phase space of the corresponding evaporation residue and the fission probability is determined by available phase space at the saddle-point on top of the fission barrier. In the case of simultaneous multifragmentation, the phase-space is explored for possible multi-fragment configurations (partitions), typically at the stage where short-range nuclear interaction freezes out and the identities of final fragments are determined.

The most commonly used phase-space model of multifragmentation, the Statistical Model of Multifragmentation (SMM) [8] implements the grand-canonical approximation, the freeze-out volume depends on fragment multiplicity and internal excitation of fragments in the freeze-out configuration is considered, thus producing "hot" fragments.

As an alternative to model of simultaneous multifragmentation, the traditional model of compound nucleus decay based on Hauser-Feshbach approximation [16] was extended to describe the emission of intermediate mass fragments (IMF) [17]. The emission of such complex fragments is described as a binary split, essentially an asymmetric fission where the IMF is accompanied by a heavy residue. The emission probability is determined by a value of the mass-asymmetric fission barrier height. The most common implementation of such model of Sequential Binary Decay (SBD) is the GEMINI code [9] which was used extensively for comparisons with experimental multifragmentation data, with reasonable success in description of e.g. inclusive mass and charge distributions. However, the model of sequential binary decay fails to describe the results of exclusive measurements at the zero angle while SMM performs rather well [18].

Collisions of ^{86}Kr+^{64}Ni at 25 AMeV

Peripheral collisions in the nearly symmetric system at beam energy within the Fermi energy domain were investigated in detail in the reaction ^{86}Kr+^{64}Ni at 25 AMeV [2] for angular acceptance of the recoil separator MARS [19] centered around 0 °. An enhancement of the yields of neutron-rich nuclei over the prediction of both simulations (PE+DIT/ICF+SMM/GEMINI) [1] and EPAX [20] systematics for fragmentation cross sections was observed and the shapes of the velocity spectra suggested a process with a short timescale such as very peripheral collisions where the details of neutron and proton density profiles at the projectile and target surfaces can play a significant role. Such excessive yields of neutron-rich nuclei can be caused by the effect of the neutron-rich surface of the target nucleus, which in peripheral collisions can lead to stronger flow of neutrons from the target to the projectile (or flow of protons in the opposite direction), thus reverting the flow toward isospin equilibration. In [21], the DIT model of Tassan-Got [7] was supplemented with a phenomenological correction introducing the effect of shell structure on the nuclear periphery.

Based on expected correlation of the $R_n - R_p$ with $\mu_n - \mu_p$, in particular considering the possibility to estimate the surface properties of real nuclei using the value of $-(S_n - S_p)$, a minor modification in the DIT code of Tassan-Got [7] was made by scaling the transfer probabilities by the exponential factors

$$\begin{aligned}
P_n(P \to T) &\longrightarrow \mathrm{e}^{-0.5\kappa(\delta S_{nP} - \delta S_{pP} - \delta S_{nT} + \delta S_{pT})} P_n(P \to T) \\
P_p(P \to T) &\longrightarrow \mathrm{e}^{0.5\kappa(\delta S_{nP} - \delta S_{pP} - \delta S_{nT} + \delta S_{pT})} P_p(P \to T) \\
P_n(T \to P) &\longrightarrow \mathrm{e}^{-0.5\kappa(\delta S_{nT} - \delta S_{pT} - \delta S_{nP} + \delta S_{pP})} P_n(T \to P) \\
P_p(T \to P) &\longrightarrow \mathrm{e}^{0.5\kappa(\delta S_{nT} - \delta S_{pT} - \delta S_{nP} + \delta S_{pP})} P_p(T \to P) \qquad (2)
\end{aligned}$$

where κ is a free parameter and δS_{nP}, δS_{pP}, δS_{nT}, δS_{pT} represent the differences of neutron and proton separation energies for the projectile and target calculated using the experimental [22] and liquid-drop [23] masses, thus expressing the effect of the microscopic structure. The smooth part is subtracted from the experimental values due to the fact that the macroscopic values of $\mu_n - \mu_p$ follow the bulk N/Z-ratios of reaction partners and the bulk N/Z equilibration is described consistently by the DIT code

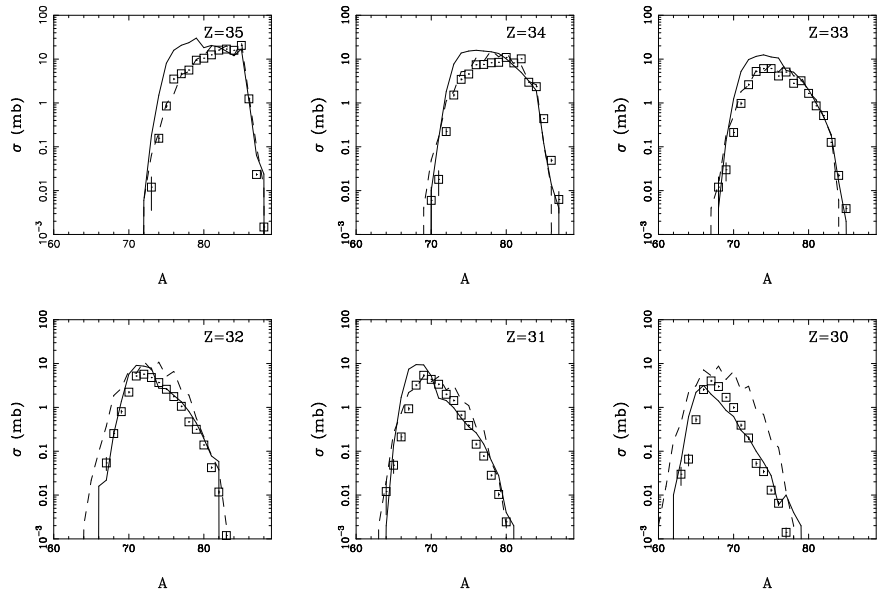

Figure 2: Experimental mass distributions (symbols) of elements with Z = 30 - 35 observed in the reaction ^{86}Kr+^{64}Ni at 25 AMeV [2] for angular acceptance centered around 0 °, compared to the results of the PE+DIT/ICF simulation with modified DIT calculations combined with the de-excitation codes SMM and GEMINI (solid and dashed line, respectively).

of Tassan-Got. Thus, the macroscopic concepts used in DIT model are supplemented with phenomenological information on shell structure at the nuclear periphery which can explain the deviation of nucleon exchange from the path toward isospin equilibration, and the model framework assumes the micro-macroscopic structure. The modified DIT calculation was used only for non-overlapping projectile-target configurations, consistent with the assumption that it represents an effect of nuclear periphery. A cut-off was set at separation representing touching half-density surfaces below which a standard DIT calculation, following the path toward isospin equilibration, was used.

In Fig. 2 we present the experimental mass distributions of elements with Z = 30 - 35 observed within the separator acceptance in the reaction ^{86}Kr+^{64}Ni at 25 AMeV [2] compared to the simulation with the modified DIT calculations, combined with the two de-excitation codes SMM [8] (full line) and GEMINI (dashed line) [9]. The simulated yields were filtered for angular

acceptance of the spectrometer MARS. Several calculations were performed with different values of κ and the value of $\kappa = 0.53$, used in the modified DIT calculations presented in Fig. 2, was obtained as an optimum value reproducing the experimental mass distributions when using both de-excitation codes, specifically for neutron-rich nuclei with Z = 35 - 32. Otherwise, the GEMINI calculation results in the nearly symmetric mass distributions which appear to overestimate the widths of mass distributions of lighter elements. The SMM calculation appears to reproduce well the yields of neutron-rich nuclei also for lighter elements, on the other hand the yields of β-stable isotopes appear to be overestimated. Such differences of GEMINI and SMM calculations are in good agreement with the results of the work [18] where the SMM calculations lead to better reproduction of yields originating from the hot quasiprojectiles, while for the colder quasiprojectiles with excitation energies 1-2 AMeV GEMINI performed better due to the implementation of sequential binary decay which is missing in the simulation of secondary emission from the hot fragments in SMM.

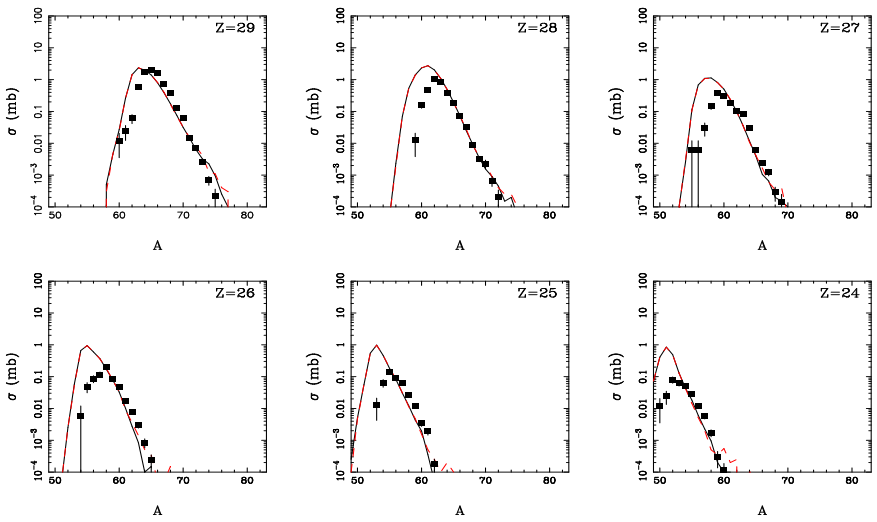

Figure 3: Experimental (symbols) and simulated (lines) mass distributions of elements with Z = 29 - 24 observed in the reaction ^{86}Kr+^{64}Ni at 25 AMeV within the separator acceptance centered around 0 °.

In Fig. 3 is shown a comparison of experimental and simulated mass distributions of elements with Z = 29 - 24 observed within the separator acceptance centered around 0 ° in the reaction ^{86}Kr+^{64}Ni at 25 AMeV [2].

For these products, originating predominantly from more violent collisions, incomplete fusion appears as dominant reaction mechanism.

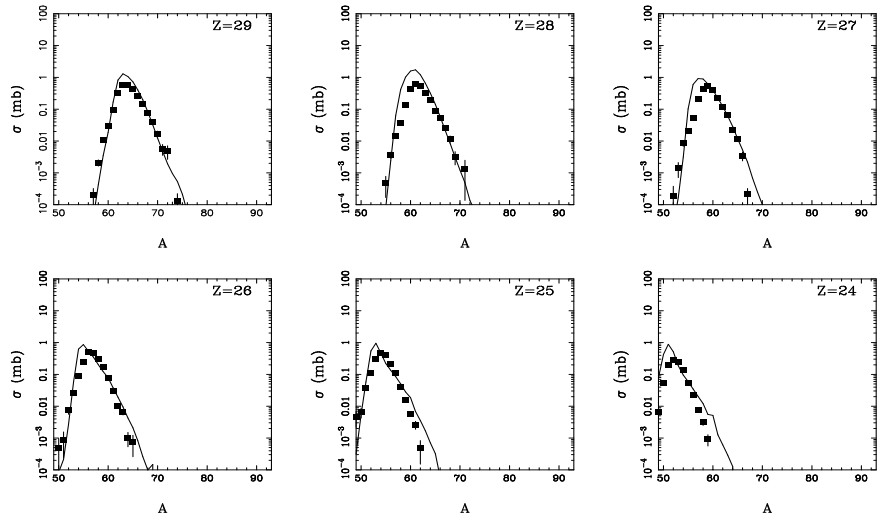

Figure 4: Experimental (symbols) and simulated (lines) mass distributions of elements with Z = 29 - 24 observed in the reaction ^{86}Kr+^{64}Ni at 25 AMeV within the separator acceptance centered around 4 °.

For the reaction ^{86}Kr+^{64}Ni at 25 AMeV, data were obtained also for angular acceptance centered around 4 °. Using the same simulation as in the previous figures, and using appropriate angular cuts reflecting both radial and azimuthal coverage, the results are shown for Z= 29 - 24 in Figure 4. Also in this case the experimental data and simulation agree reasonably, thus the simulation appears to describe the production cross sections also at angles away from zero.

Collisions of ^{86}Kr+^{112,124}Sn at 25 AMeV

Figure 5 shows the experimental mass distributions of elements with Z = 30 - 35 observed in the reaction ^{86}Kr+^{124}Sn at 25 AMeV [3] compared to the results of the PE+DIT/ICF simulation with the modified DIT model (as in the case of ^{86}Kr+^{64}Ni at 25 AMeV) combined with the SMM (full line) and GEMINI (dashed line). The simulated yields were filtered for angular acceptance of the separator positioned at 4° (covering polar angles

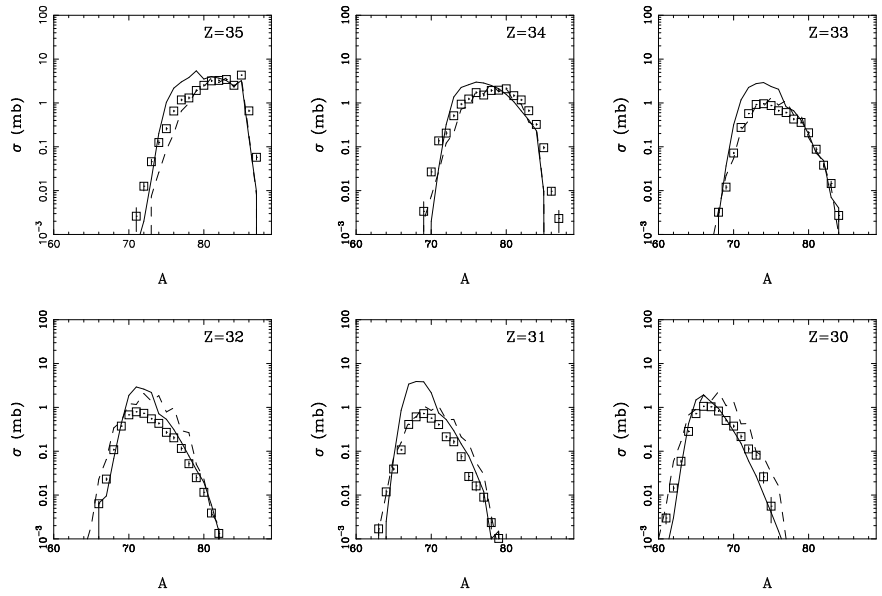

Figure 5: Experimental mass distributions (symbols) of elements with Z = 30 - 35 observed in the reaction ^{86}Kr+^{124}Sn at 25 AMeV [3] compared to the results of the PE+DIT/ICF simulation with the modified DIT model with SMM (full line) and GEMINI (dashed line).

2.7 - 5.4 ° [3]) with appropriate azimuthal corrections. One can see that in this case, the overall agreement with the experimental data is improved by the modified DIT calculation (using $\kappa = 0.53$ as in the previous case). As in the previous case, the modified DIT calculation with SMM appears to reproduce the shapes of mass distributions more consistently (except the overestimation of the yields of β-stable nuclei), while the GEMINI code appears to lead to more symmetric mass distributions with overestimated width at lower atomic numbers.

Fig. 6 presents the experimental mass distributions of elements with Z = 30 - 35 observed in the reaction ^{86}Kr+^{112}Sn at 25 AMeV [3], again compared to the results of the simulation with the modified DIT calculations combined with the SMM (dhash-dotted line) and GEMINI (dashed line). In this case the modified DIT calculation (using the value $\kappa = 0.53$ successful in previous cases) combined with GEMINI leads to improvement for Z = 35 - 34, consistent with previous cases. However, the simulation with modified DIT calculation combined with GEMINI appears to overestimate the yields

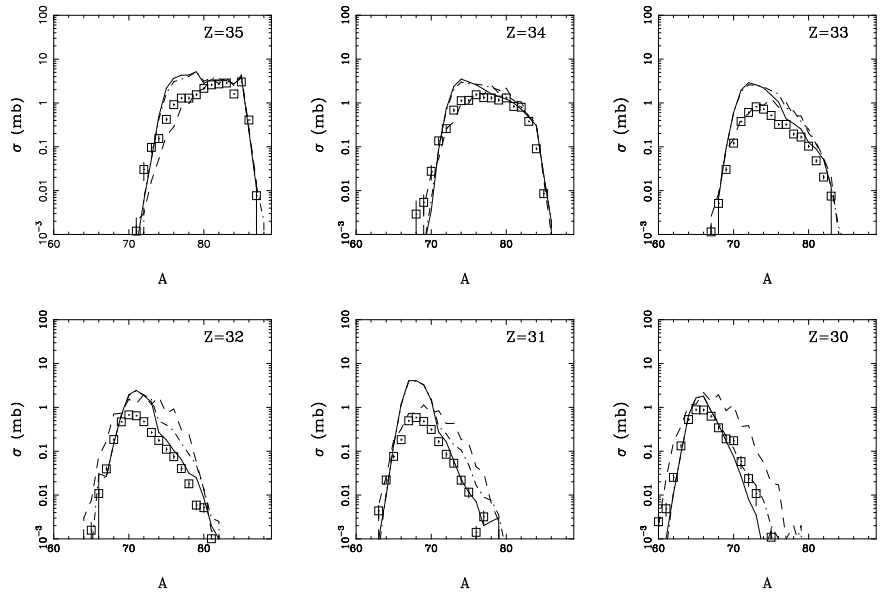

Figure 6: Experimental mass distributions (symbols) of elements with Z = 30 - 35 observed in the reaction ^{86}Kr+^{112}Sn at 25 AMeV [3] compared to the results of the simulation with the modified DIT model with SMM (dash-dotted line) and GEMINI (dashed line). Solid line represents the modified DIT with a cutoff shifted to 0.8 fm combined with SMM.

of neutron-rich nuclei with Z = 33 - 30 due to shifted centroids and overestimation of both maximum value and width. The modified DIT calculation combined with SMM appears to reproduce the shapes of mass distribution consistent to previous cases, well at the neutron-rich side (specifically for the Z = 35 - 34), while overestimating the yields of β-stable nuclei. For Z = 33 - 31 the overall elemental yields appear to be overestimated. Such a situation in the reaction ^{86}Kr+^{112}Sn may signal that an increase of proton transfer probability into the massive proton-rich target according to Eqn. (2) may be reverted at smaller separation distances by the effect of increasingly repulsive Coulomb interaction. The solid line in Fig. 6 represents simulation with modified DIT calculation ($\kappa = 0.53$) where the cut-off is shifted to minimal separation of half-density surfaces equal to 0.8 fm, again combined with SMM. Such a simulation reproduces the experimental mass distributions much better, thus suggesting that for the proton-rich target ^{112}Sn, the proton transfer barrier assumes its sensitivity to isospin asymmetry of nu-

clear periphery 0.8 fm outwards when compared to neutron-rich targets, due to the effect of stronger Coulomb repulsion at more compact di-nuclear configurations than predicted by the approximation used.

According to the incomplete fusion model [1], the cold fragmentation-like residues should be increasingly dominant products for the channels with the number of stripped protons exceeding seven to eight. Thus the products of primary interest are the heavy residues considerably lighter than the initial projectile, which due to the removal of a significant number of protons can be also considerably neutron-rich.

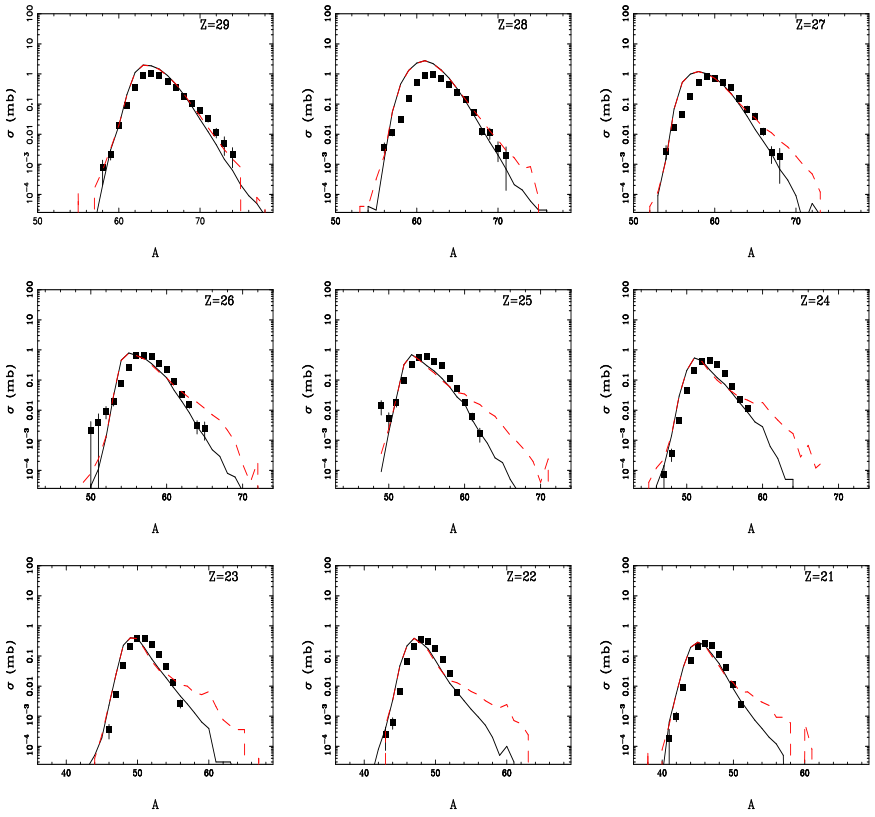

Figure 7: Comparison of the simulations to experimental mass distributions (symbols) of elements with Z = 21 - 29 observed around 4° in the reaction ^{86}Kr+^{124}Sn at 25 AMeV [3]. Dashed line - results of the standard simulation [1, 21] combined with the de-excitation code SMM [8], Solid line - results of simulation using modified model of incomplete fusion (eq. (3)).

In order to examine the prediction of the ICF model [1], the results of simulations were compared to experimental mass distributions of elements with Z = 21 - 29 observed in the reaction ^{86}Kr+^{124,112}Sn at 25 AMeV [3]. Figs. 7, 8 show the comparison of experimental mass distributions (symbols) to the results of the simulation (dashed line). The simulation uses either the model of deep-inelastic transfer [7, 21] for peripheral collisions or the model of incomplete fusion (ICF) for violent (central) collisions, combined with the de-excitation code SMM [8]. The simulated yields were filtered for angular acceptance of the separator positioned at 4° with appropriate azimuthal corrections [3]. One can see that for the reaction ^{86}Kr+^{124}Sn the calculation overpredicts the experimental yields of the most neutron-rich products below nickel (with more than 8 stripped protons). The situation is similar also for the reaction ^{86}Kr+^{112}Sn even if the most neutron-rich products below nickel are less populated than in reaction of ^{86}Kr+^{124}Sn. Thus the yields of neutron-rich nuclei appear to be overpredicted in the region where the cold fragmentation-like residues dominate.

The model of incomplete fusion [1], used in the calculation, considers a spectator-participant scenario evolving along the classical Coulomb trajectory, followed by fusion of the participant zone with one spectator, typically the heavier one due to larger contact area and thus larger attractive force. The charge of spectator zones is determined using the combinatorial probability, which is a standard approach in fragmentation codes [14]. The excitation energy of the cold fragment is determined considering the two-body collisions of participant and spectator nucleons along the separation plane [1]. The concept of combinatorial probability explores the available statistical phase space and allows a rather wide range of isospin asymmetries. From a dynamical point of view, however, the spectator-participant scenario implies an instantaneous separation and thus preservation of isospin asymmetry of the initial nucleus in the ground state, with homogeneous density in the interior of the nucleus. The two concepts seem to be in contradiction, which can be resolved when assuming that the change of isospin asymmetry is dynamically consistent with transfer of certain amount of nucleons across the separation plane. Simultaneously, the relative velocity between the participant and spectator zone increases from zero to maximum value corresponding to final incomplete-fusion scenario and the transferred nucleons should carry this relative velocity which will be transferred into excitation energy of the acceptor. Thus a component of excitation energy dependent on isospin asymmetry can be deduced. It can be assumed that, due to absence of Coulomb

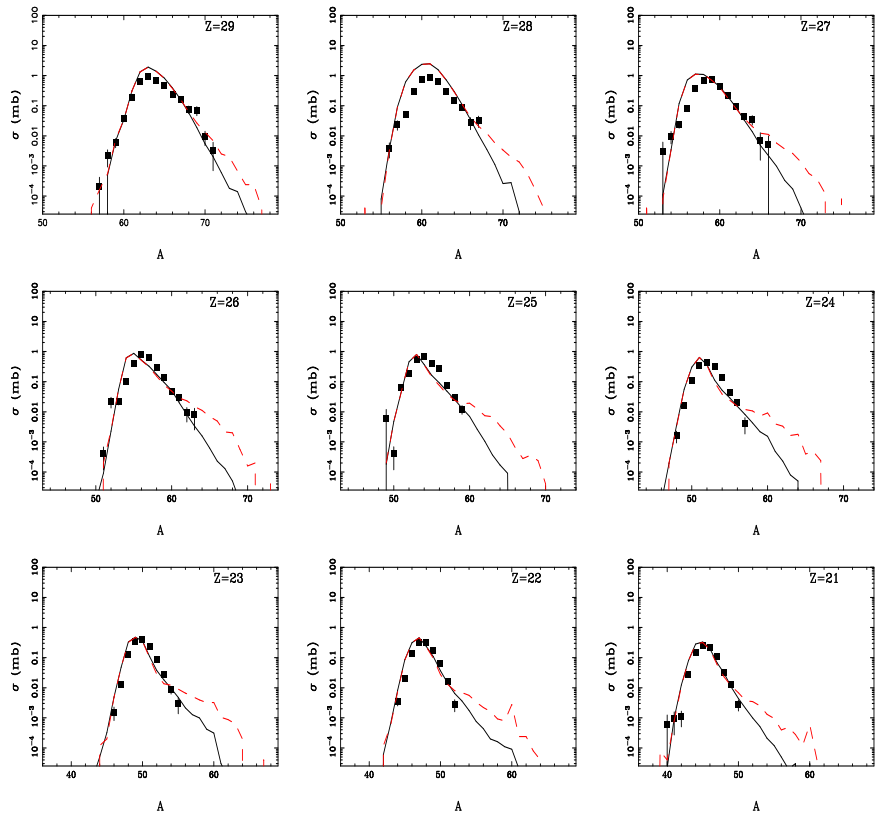

Figure 8: Comparison of the simulations to experimental mass distributions (symbols) of elements with Z = 21 - 29 observed around 4° in the reaction ^{86}Kr+^{112}Sn at 25 AMeV [3]. Solid, dashed lines - as in Fig. 7.

barrier, the nucleons transferred will be predominantly neutrons. The formula for such isospin dependent component of excitation energy of a cold spectator (acceptor) can be written as

$$E^*_S(A_S, Z_S) = x\ (A_S - A_0(Z_S))\ (\frac{v^{ICF}_{rel}}{v_{proj}})^2\ \frac{E_P - V_C}{A_P} \qquad (3)$$

where E_P, A_P are the projectile kinetic energy and mass, V_C is the Coulomb barrier, v_{proj}, v^{ICF}_{rel} are the projectile velocity and the final relative velocity between hot and cold fragment in the incomplete-fusion scenario, evaluated at the Coulomb barrier, A_S, Z_S are mass and charge of the spectator (cold fragment), $A_0(Z_S)$ is the spectator mass corresponding to N/Z

of initial nucleus and x is a random number between zero and one, generated for each collision. The random number is introduced due to uncertainty concerning the exact moment of transfer and represents an zero-th order estimate allowing to reproduce the mean value of extra excitation energy due to transfer of neutrons.

The results of modified calculation employing the formula (3) are shown in Figs. 7, 8 as solid lines. One can see that overall agreement with the experimental data is improved in the modified calculation compared to the standard one. The situation improves also for the reaction ^{86}Kr+^{112}Sn. For the most neutron-rich products below chromium nuclei occasionally appear less populated than it is predicted by the model. This however can be caused by missing yield in the experiment due to background from the initial beam, because of increasing overlap of the charge states (in terms of magnetic rigidity) with charge states of the scattered beam. The effect is more pronounced for the reaction ^{86}Kr+^{112}Sn due to lower experimental yields.

In general, the modifications in the model of incomplete fusion appear consistent with both overall model framework and experimental data and thus one can expect improved predictive power which can be used to predict production of exotic mid-heavy to heavy neutron-rich nuclei in the reactions around the Fermi energy, and possibly identify under which conditions such approach can be more effective than other methods. From the point of view of reaction dynamics, the modified model of incomplete fusion is consistent with the formation of a neutron-rich region between cold and hot fragment (or participant zone as its precursor). Similar effect was reported in the literature [24] as a possible consequence of the evolution of nuclear mean field. The number of transferred neutrons can then be determined by a mechanism similar to the random neck rupture, as established in nuclear fission [25], which can justify the applicability of a combinatorial (and thus essentially statistical) probability in the description of dynamical reaction mechanism such as the incomplete fusion.

Collisions of ^{124}Sn+^{124}Sn at 20 AMeV

Also in another reaction of massive heavy ions ^{124}Sn+ ^{124}Sn [26] at 20 AMeV, an enhancement was observed over the yields expected in cold fragmentation (as represented by EPAX [20] estimates).

In this reaction, reaction products up to krypton were isotopically resolved. Such products are considerably lighter than the projectile and thus

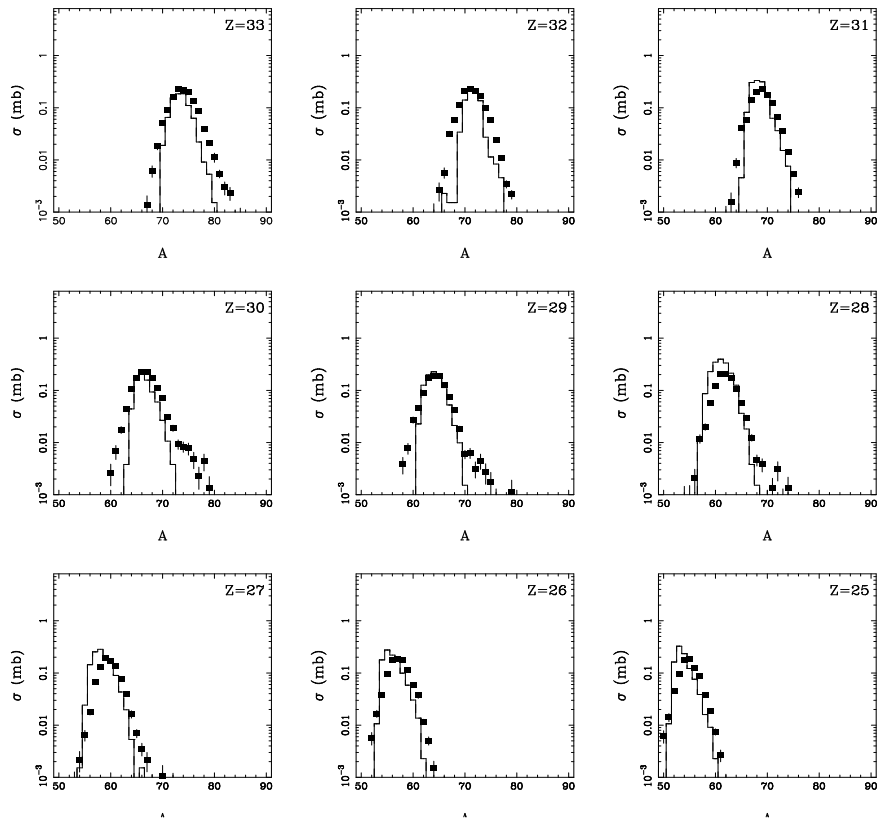

Figure 9: Comparison of the simulated (solid lines) to experimental mass distributions (symbols) of elements with Z = 25 - 33 observed at 0° in the reaction ^{124}Sn+^{124}Sn at 20 AMeV [26].

more central collisions where incomplete fusion of the participant zone with either projectile or taget participant occurs should be contributing dominantly. Figure 9 shows that the observed yields are again reproduced reasonably well using the same simulation as in the Figures 7, 8. The simulated yields were filtered for angular acceptance of the MARS recoil separator positioned at 0° (covering polar angles up to 3 ° [26]). Thus one can conclude that nearly symmetric reactions of massive heavy ions at beam energies around 20 - 30 AMeV are understood in terms of reaction mechanism. This allows to explore other beam energy and reaction asymmetry combinations.

Collisions of ^{129}Xe+^{197}Au,^{90}Zr at 44 AMeV

Another reaction of massive heavy ions ^{129}Xe+^{197}Au at 44 AMeV was investigated by authors of the work [27]. Projectile-like residues were observed at forward angles. This reaction represents a typical reaction in normal kinematics at beam energy close to the upper limit of the Fermi energy domain.

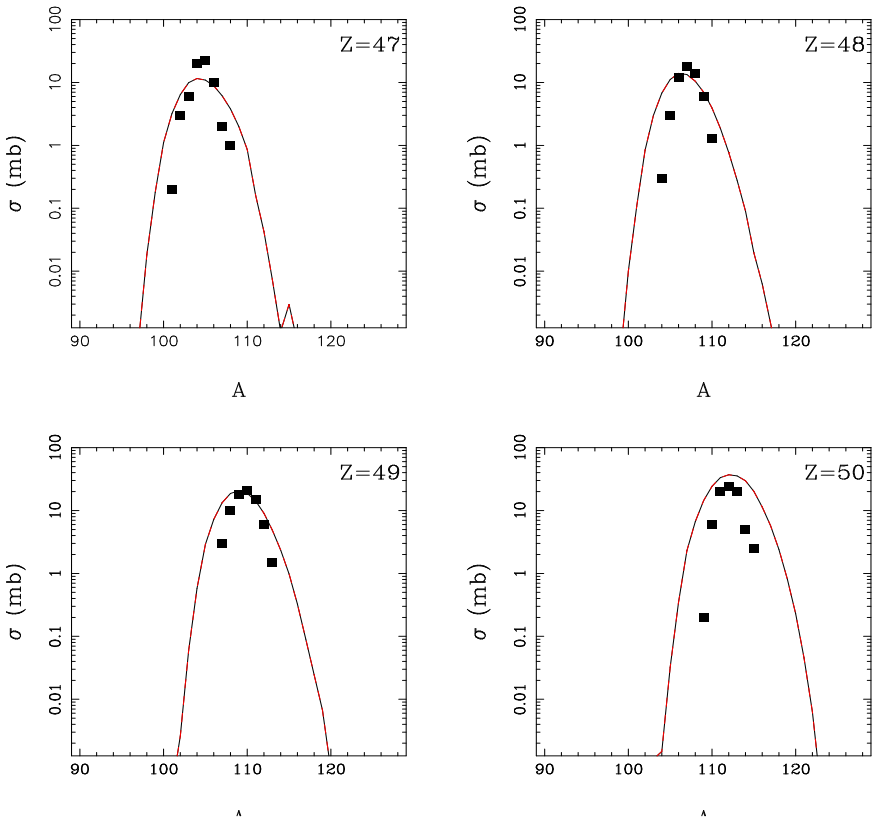

Figure 10: Comparison of the simulations (solid lines) to experimental mass distributions (symbols) of elements with Z = 47 - 50 observed at 0° in the reaction ^{129}Xe+^{197}Au at 44 AMeV [27].

Figure 10 shows that the observed yields are again reproduced reasonably well using the same simulation as in the Figures 7, 8, 9. The simulated yields were filtered for angular acceptance of the separator SPEG [28] positioned at 3° [27]. Thus one can conclude that also this reactions of massive heavy ions at beam energies below 50 AMeV is understood in terms of reaction

mechanism.

The authors of the work [27] investigated also reaction of nearly symmetric heavy ions ^{129}Xe+^{90}Zr at 44 AMeV. Identical set of projectile-like residues was observed at forward angles.

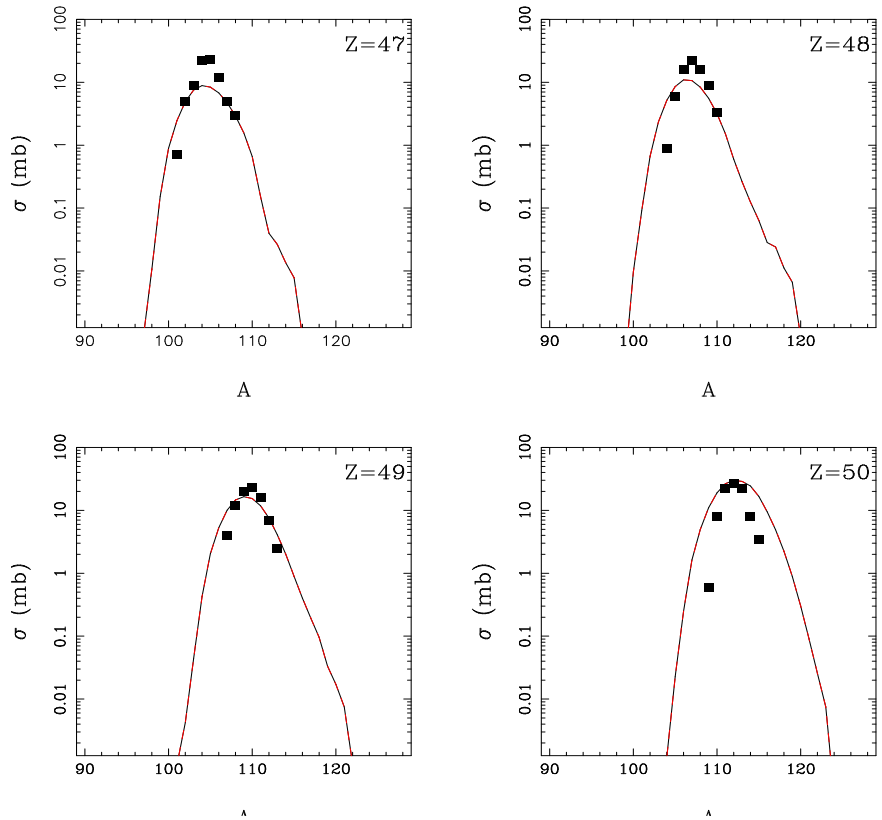

Figure 11: Comparison of the simulations (solid lines) to experimental mass distributions (symbols) of elements with Z = 47 - 50 observed at 0° in the reaction ^{129}Xe+^{90}Zr at 44 AMeV [27].

Figure 11 shows that the observed yields are again reproduced reasonably well using the same simulation as in the Figures 7, 8, 9. The simulated yields were filtered as in the previous case. Thus also this reactions of massive heavy ions at beam energies below 50 AMeV can be considered as understood in terms of reaction mechanism.

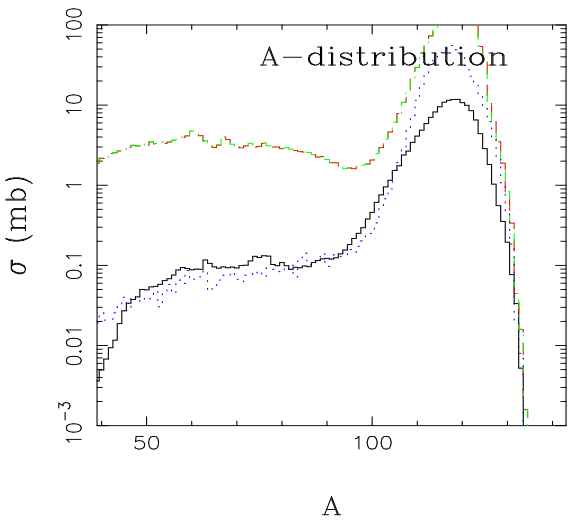

Figure 12: Experimental (solid line) and simulated mass distributions in the reaction ^{124}Sn+^{27}Al at 20 AMeV. Dotted line - PE+DIT/ICF+SMM simulation after the filtering procedure taking into account angular acceptance of the MARS spectrometer. Dashed line - an estimate of the total residue cross sections.

Collisions of ^{124}Sn+^{27}Al at 20 AMeV

Projectile-like products up to the krypton were investigated in another reaction of massive heavy ion beam ^{124}Sn with light target nucleus ^{27}Al at 20 AMeV [18] with the recoil separator MARS positioned at 0°. This reaction is a typical case of the reaction in inverse kinematics at beam energy around the lower edge of the region of energies comparable to the Fermi energy. Figure 12 shows experimental (solid line) and simulated mass distributions. The PE+DIT/ICF simulation (dotted line) allows to reproduce well the experimental mass distibution, after the proper filtering procedure taking into account angular acceptance of the MARS spectrometer. Dashed line shows an estimate of the total residue cross sections.

Figure 13 shows similar comparison for mass distributions of selected elements between iron and krypton. Again the filtered simulation (solid line) reproduces well the experimental data (symbols), with some discrepancies possibly due to low statistics. The estimated unfiltered isotopic yields (dashed lines) are compared to estimates by the systematics EPAX [20] (dotted lines). EPAX appears to overestimate the unfiltered yields, since

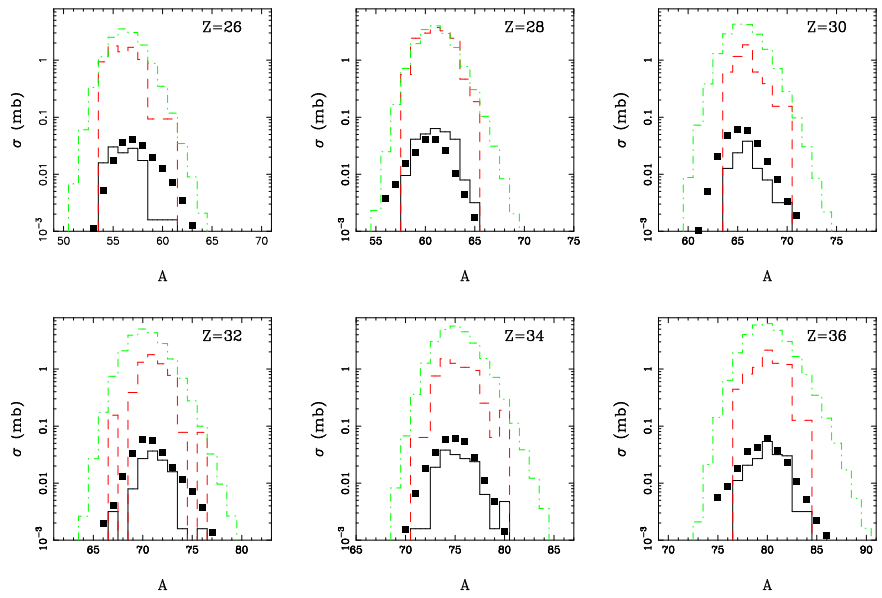

Figure 13: Experimental (symbols) and simulated (lines) mass distributions in the reaction ^{124}Sn+^{27}Al at 20 AMeV for selected elements between iron and krypton. Solid line - PE+DIT/ICF+SMM simulation after the filtering procedure taking into account angular acceptance of the MARS spectrometer. Dashed line - an estimate of the total residue cross sections. Dotted line - an estimate by the EPAX [20].

the incomplete fusion mechanism tends to concentrate yields closer to the projectile mass.

Collisions of ^{129}Xe+^{27}Al at 26 AMeV

The reaction of massive heavy ions ^{129}Xe with light target ^{27}Al was investigated in the work [29] at beam energy 26 AMeV . Projectile-like residues were observed at forward angles using the spectrometer A1200 [30]. This reaction is similar to the previous one and thus one can expect that the dominant reaction mechanism will be similar. In Figure 14 the filtered simulation (solid line), analogous to the previous case, reproduces reasonably well the experimental data (symbols), with some discrepancies possibly caused by uncertainty due to presentation of experimental data in the work [29] or by simple filtering procedure roughly approximating the angular acceptance of the spectrometer A1200 in the experiment [29].

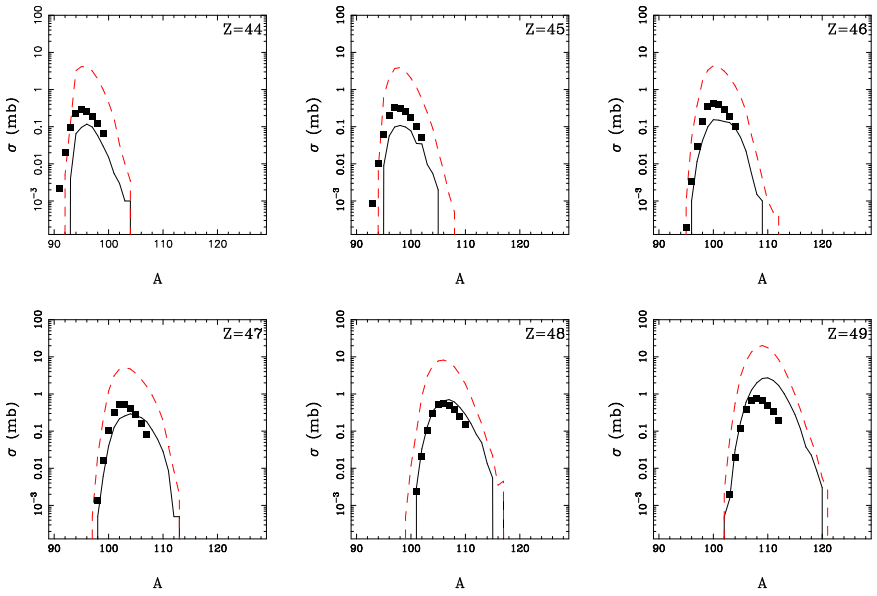

Figure 14: Experimental (symbols) and simulated (lines) mass distributions in the reaction ^{129}Xe+^{27}Al at 26 AMeV for selected elements between iron and krypton. Solid line - PE+DIT/ICF+SMM simulation after filtering procedure taking into account angular acceptance of the A1200 spectrometer [30]. Dashed line - non-filtered PE+DIT/ICF+SMM simulation.

Collisions of ^{129}Xe+^{27}Al at 50 AMeV

The reaction of massive heavy ions ^{129}Xe with light target ^{27}Al was investigated in the work [29] also at beam energy 50 AMeV around the upper limit of the definition of the Fermi energy domain. In Figure 15 the filtered simulation (solid line), with filtering procedure analogous to the previous case, fails to reproduce the experimental data, both in terms of magnitude and neutron excess (symbols).

A possible explanation for the failure of the PE+DIT/ICF simulation can be a transition from the binary DIT/ICF scenario to ternary participant-spectator scenario. To test this hypothesis the ICF model was modified so that both spectators remain cold, gaining excitation energy and kinematic properties in the same way as the cold fragment in the binary ICF scenario. Simulation using this model was performed and an improvement was achieved in terms of magnitude, however the shift in the isospin, with experimental data being less neutron-rich, remained practically unchanged. It

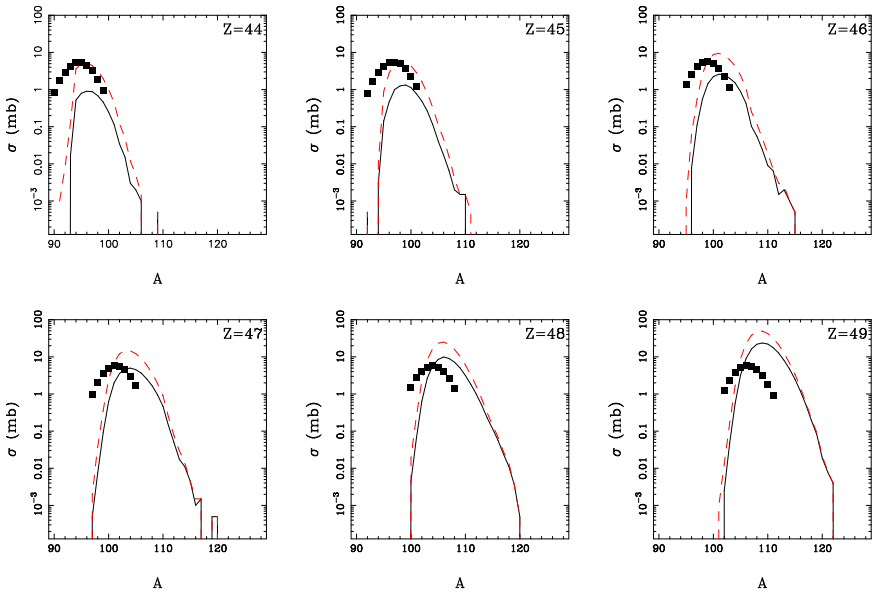

Figure 15: Experimental (symbols) and simulated (lines) mass distributions in the reaction ^{129}Xe+^{27}Al at 50 AMeV for selected elements between iron and krypton. Solid line - PE+DIT/ICF+SMM simulation after filtering procedure taking into account angular acceptance of the A1200 spectrometer. Dashed line - non-filtered PE+DIT/ICF+SMM simulation.

is de-facto excluded that the isospin shift could be caused by de-excitation stage, since in the same reaction at lower beam energy 26 AMeV and in the reactions ^{129}Xe+^{197}Au,^{90}Zr at 44 AMeV, with similar projectile-like source and excitation energies, no such shift is observed. Thus the shift is caused by the dynamical stage. One possible cause of the shift can be in the mechanism of dynamical emission of neutrons, as recently reported in the work [5]. If such emission takes place during the re-separation, a significant shift toward proton-rich side can be achieved. Such assumption was tested by a modified participant-spectator simulation (solid line) where six neutrons (which corresponding decrease of excitation energy) were subtracted from the projectile-like spectator. This simulation leads to reasonable agreement with experimental data, thus suggesting that mean field effects in the re-separation stage can influence the production cross sections of heavy residues, primarily in proton-rich systems.

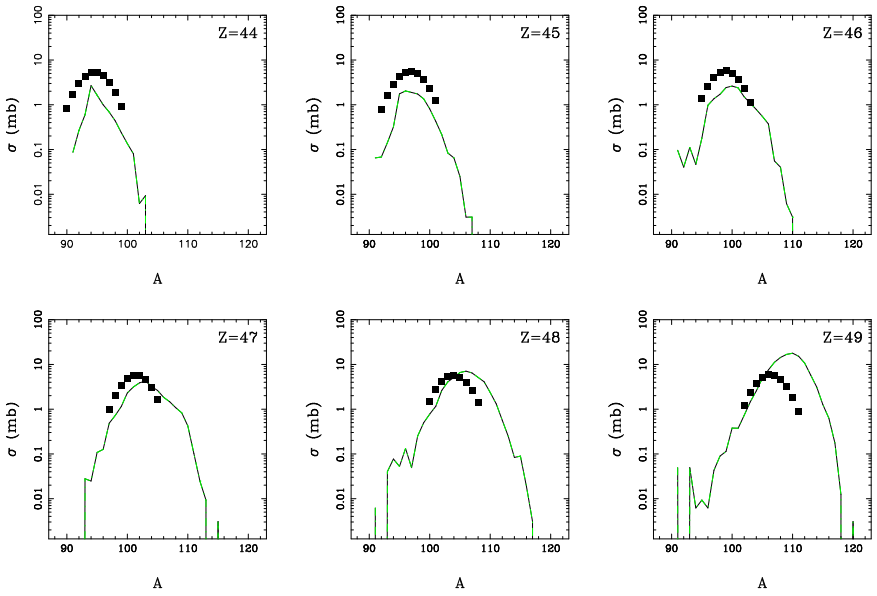

Figure 16: Experimental (symbols) and simulated mass distributions in the reaction ^{129}Xe+^{27}Al at 50 AMeV for selected elements between iron and krypton. Lines represent the PE+participant-spectator+SMM simulation after filtering procedure taking into account angular acceptance of the A1200 spectrometer and subtraction of six neutrons prior to de-excitation.

Collisions of ^{86}Kr+^{27}Al at 70 AMeV

A test of the onset of the participant-spectator scenario can be provided by the reaction of ^{86}Kr beam with light target ^{27}Al which was investigated in the work [31] at beam energy 70 AMeV, above the Fermi energy domain. As can be seen in Figure 17, the filtered participant-spectator simulation (solid line), with filtering procedure approximating the angular acceptance of the spectrometer A1200 [30] used in the experiment [31], appears to reproduce the experimental data below the projectile (symbols). It is however worthwhile to note that the PE+DIT/ICF simulation is successful below the projectile and works better at elements heavier than the projectile. This observation puts into question the definition of the energy range above 50 AMeV as a fragmentation domain.

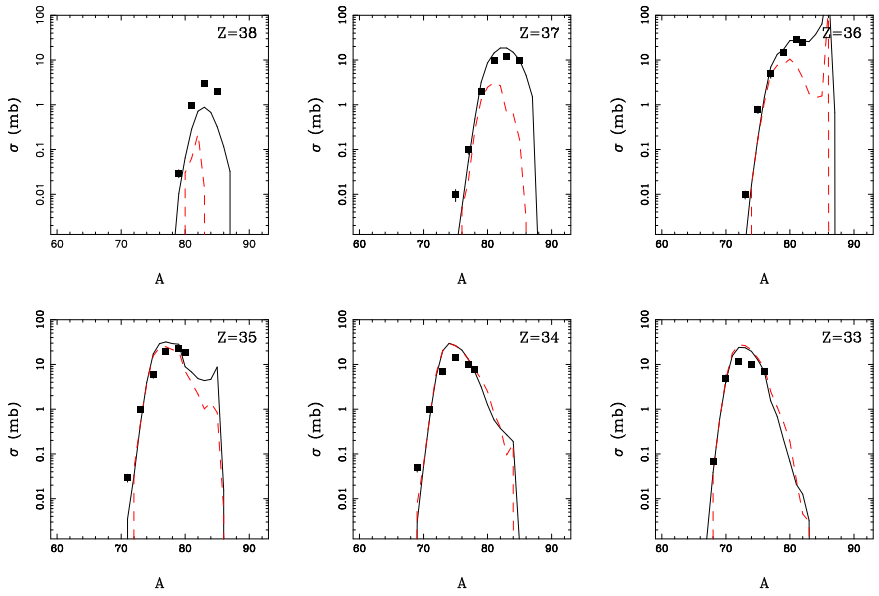

Figure 17: Experimental (symbols) and simulated (lines) mass distributions in the reaction ^{86}Kr+^{27}Al at 70 AMeV for selected elements. Solid line - PE+participant-spectator+SMM simulation after filtering procedure taking into account angular acceptance of the A1200 spectrometer. Dashed line - PE+DIT/ICF+SMM simulation after filtering procedure.

Collisions of ^{78}Kr+^{58}Ni at 75 AMeV

Futher test of the onset of the participant-spectator scenario can be provided by the reaction of ^{78}Kr beam with target ^{58}Ni which was investigated in the work [32] at beam energy 75 AMeV, again above the Fermi energy domain. As can be seen in Figure 18 the filtered participant-spectator simulation (solid line), with filtering procedure approximating the angular acceptance of the spectrometer A1200 as used in the experiment [32], comprehensively fails to reproduce the experimental data (symbols).

Figure 19 shows that the filtered PE+DIT/ICF+SMM simulation (solid line), with filtering procedure approximating the angular acceptance of the spectrometer A1200, appears to reproduce the magnitude of the cross section in the experimental data (symbols). There still remains shift in the isospin of the heavy residues, similar to the reaction ^{129}Xe+^{27}Al at 50 AMeV. Also in this case improvement was achieved by subtracting neutrons prior to

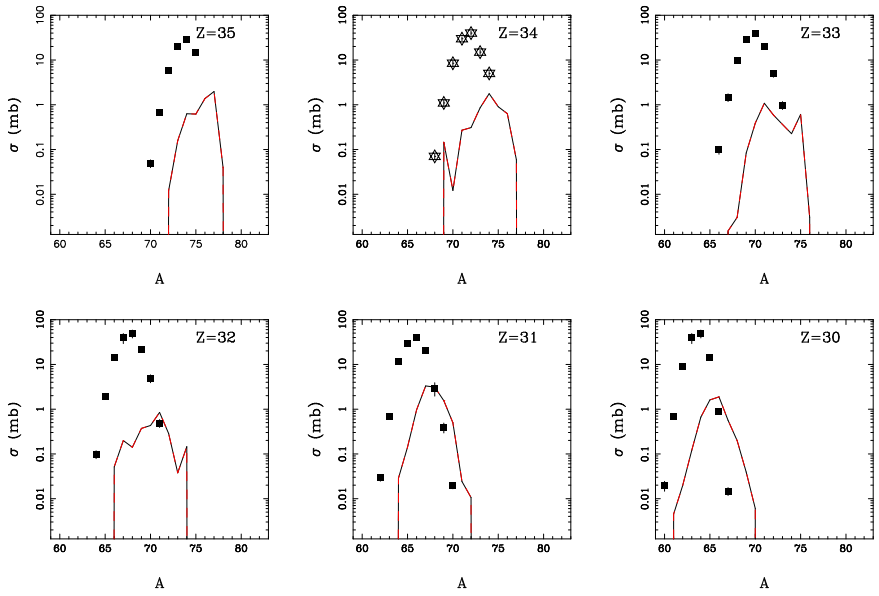

Figure 18: Experimental (symbols) and simulated (lines) mass distributions in the reaction ^{78}Kr+^{58}Ni at 75 AMeV for selected elements. Solid line - PE+participant-spectator+SMM simulation after filtering procedure taking into account angular acceptance of the A1200 spectrometer.

de-excitation, in this case four of them, as is documented in Figure 18 by the dashed lines. Thus again an isospin-dependent mechanism of dynamical emission of neutrons can play role.

Collisions of ^{86}Kr+^{181}Ta at 64 AMeV

Based on previous analysis, the reaction ^{86}Kr+^{181}Ta at 64 AMeV, in normal kinematics at energies above Fermi energy domain, can be expected as a case where PE+DIT/ICF simulation will perform well. This is documented in Figure 20, where the filtered PE+DIT/ICF simulation (solid line), with filtering procedure approximating the angular acceptance of the spectrometer RIPS [34], appears to reproduce the experimental data (symbols) quite well. Again in this neutron-rich case, there is no need to correct for the isospin shift by subtraction of neutrons, thus suggesting that in neutron-rich systems such emission either does not exist or is indistinguishabe from intense emission of neutrons in the de-excitation stage.

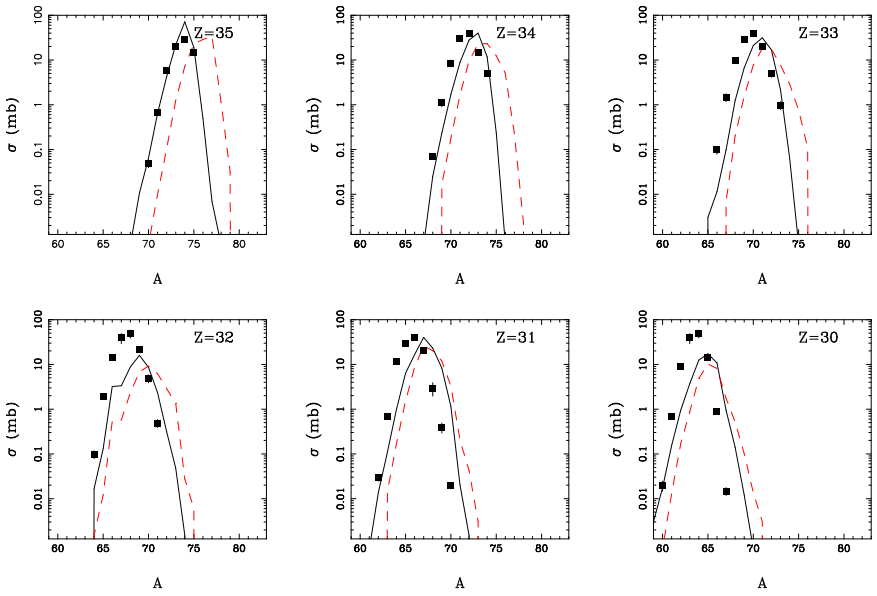

Figure 19: Experimental (symbols) and simulated (lines) mass distributions in the reaction ^{78}Kr+^{58}Ni at 75 AMeV for selected elements. Solid line - PE+DIT/ICF+SMM simulation after filtering procedure taking into account angular acceptance of the A1200 spectrometer. Dashed line - PE+DIT/ICF+SMM simulation after subtraction of four neutrons and filtering procedure.

Collisions of ^{58}Ni+^{208}Pb at 5.66 AMeV

Due to experimental difficulty, it is largely unexplored how the production mechanisms of projectile-like nuclei evolve at low beam energies down to the Coulomb barrier. Some experimental data for reactions of massive nuclei exist at energies just above the Coulomb barrier, with significant cross sections. It is of interest to establish whether such multinucleon transfer reactions can be explained within the same model framework as the nucleon exchange at Fermi energies. An attempt was undertaken to test the model framework used in the Fermi energy domain at the energies close to Coulomb barrier. It was established that using the original code the production cross sections of multi-nucleon transfer could not be reproduced. It was necessary to modify the parametrization of the nucleon density profile to allow opening of the transfer window at larger separation distances. Using the modified parameters of the trapezoidal density profile (maximum full density radius

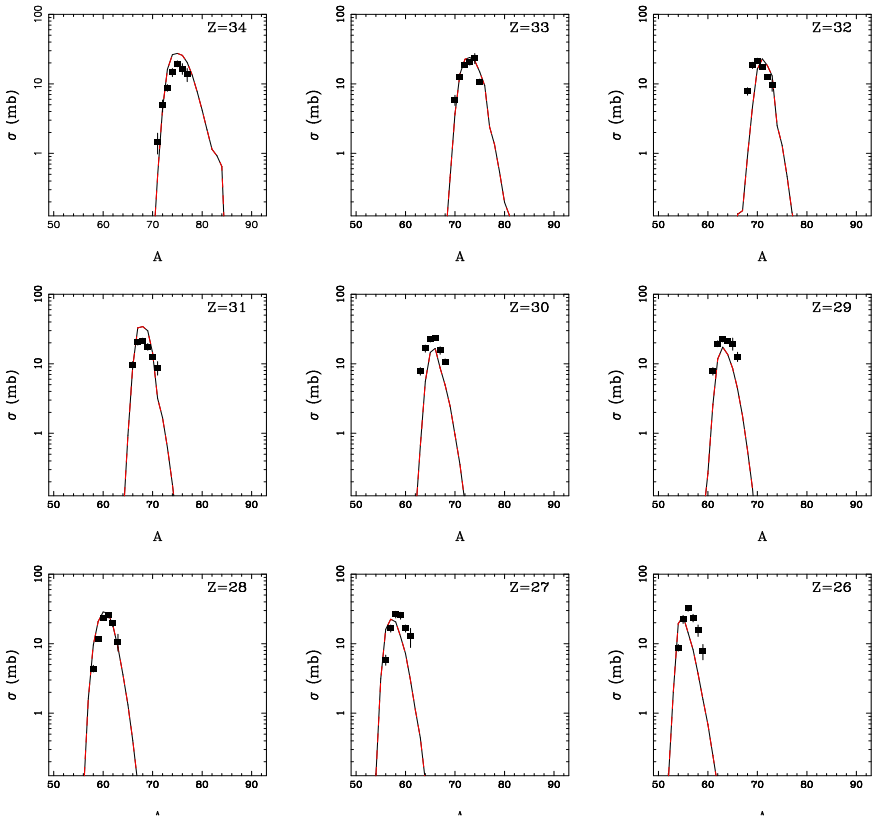

Figure 20: Experimental (symbols) and simulated (lines) mass distributions in the reaction ^{86}Kr+^{181}Ta at 64 AMeV for selected elements. Solid line - PE+DIT/ICF+SMM simulation after filtering procedure taking into account angular acceptance of the RIPS spectrometer.

R_0 enlarged by 0.7 fm and the slope increased from 0.65 to 2.2 fm), it was possible to reproduce reasonably well the cross sections of the multinucleon transfer in the reaction ^{58}Ni+^{208}Pb at 5.66 AMeV [35], as documented in the Figure 21. The necessary extension of the nuclear density profile can be possibly interpreted as a mean field effect due to evolution of the low density nuclear matter structure in the window (neck) region in the initial stage of the reaction. This explanation can provide an alternative to the initially suggested enhancement of the di-proton transfer [35].

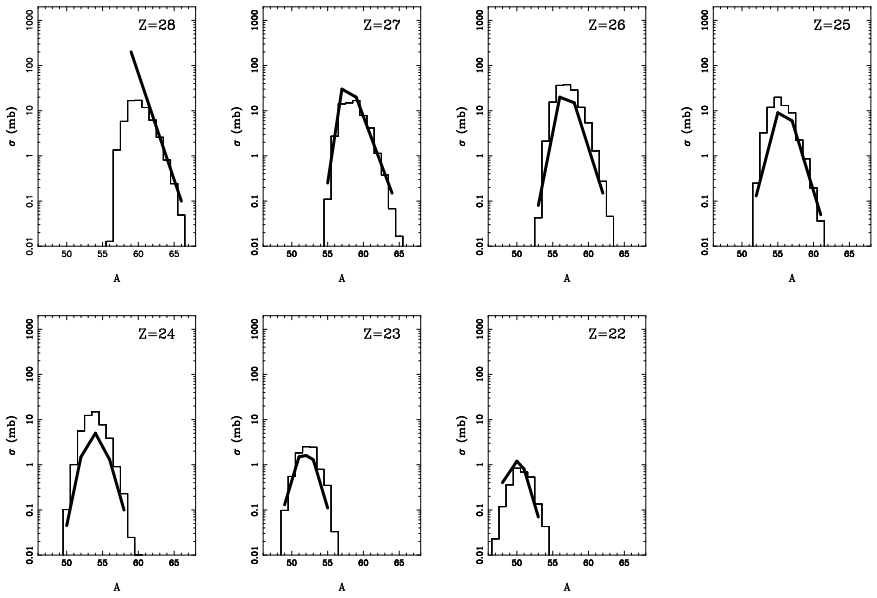

Figure 21: Experimental [35] (thick lines) and simulated (lines) mass distributions in the reaction ^{58}Ni+^{208}Pb at 5.66 AMeV for selected elements.

Collisions of ^{64}Ni+^{208}Pb at 5.47 AMeV

Another reaction with available experimental data is ^{64}Ni+^{208}Pb at 5.47 AMeV [36] where an analogous simulation was carried out with the same parameters as in the previous case. The result is shown in the Figure 22, and the agreement is analogous to the previous case. It appears that the extension of the nuclear density profile can be an effect caused by long reaction timescale at energies just above the Coulomb barrier and thus its evolution can be deterined dominantly by the initial energy of the beam.

Collisions of ^{64}Ni+^{238}U at 6.09 AMeV

The investigation of the reaction just above the Coulomb barrier was further extended to the reaction ^{64}Ni+^{238}U at 6.09 AMeV [37] and the results of identical simulation as in the previous two cases are shown in the Figure 23. Again the level of agreement is reasonably good, what supports the assumption that the necessary extension of the nuclear profile can be related dominantly to the initial energy of the beam.

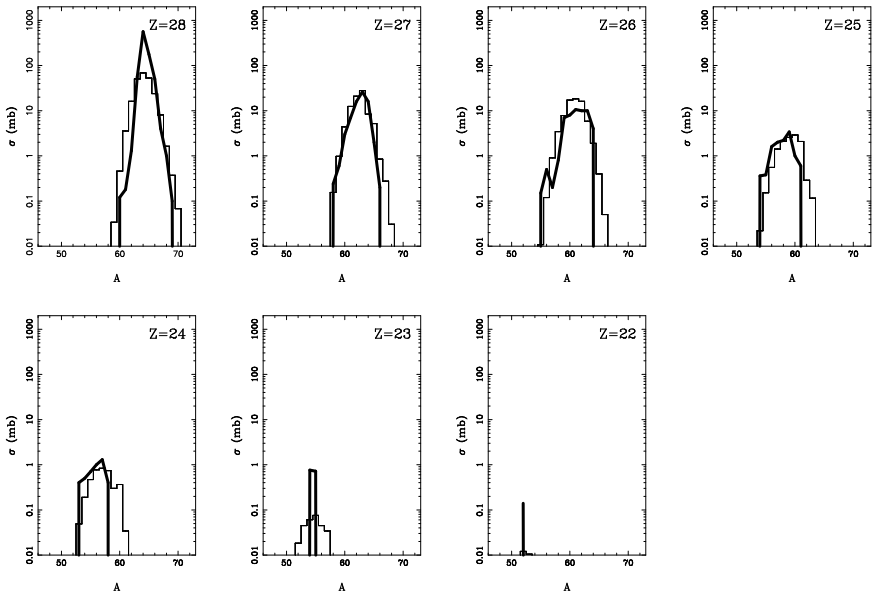

Figure 22: Experimental [36] (thick lines) and simulated (lines) mass distributions in the reaction ^{64}Ni+^{208}Pb at 5.47 AMeV for selected elements.

Collisions of ^{22}Ne+^{232}Th at 7.9 AMeV

In the context of possible mean field effect such as above mentioned extension of the nuclear profile and specifically assumption that it can be related dominantly to the initial energy of the beam, it is of interest to investigate data also at somewhat higher initial beam energy. Projectile-like nuclei were observed in the reaction ^{22}Ne+^{232}Th at beam energy 7.9 AMeV, using two detectors positioned at 12 and 40 degrees [38].

The comparisons of the observed isotopic yields (symbols) at the two angles with the results of a standard PE+DIT/ICF+SMM simulation (dashed lines) and of the version using the DIT code with the extension of the nuclear profile (solid lines) are shown in Figures 24, 25. The extension of the nuclear profile amounted to approximately 75 % compared to the three reactions at beam energy 5.5 – 6.0 AMeV. Again the standard PE+DIT/ICF+SMM simulation underpredicts the magnitude of the observed cross sections and improvement is achieved when using the extended nuclear profile, with the necessary extension weaker by 25% than in reactions at lower beam energy. Thus it appears that there exists a trend where the magnitude of extension

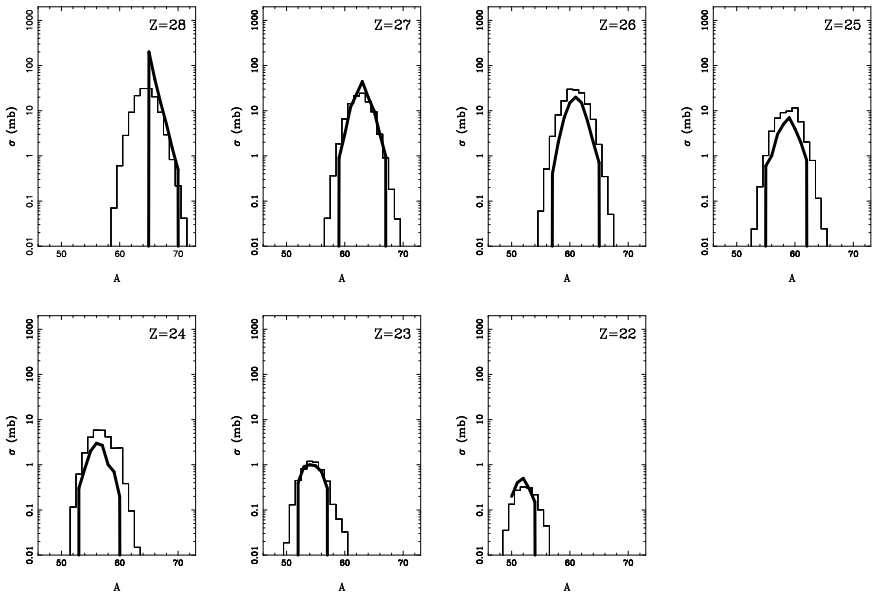

Figure 23: Experimental [37] (thick lines) and simulated (lines) mass distributions in the reaction ^{58}Ni+^{208}Pb at 6.09 AMeV for selected elements.

decreases with beam energy, possibly due to shorter collision time. Reasonable agreement is reached at 40 degrees, while at 12 degrees there appears a problem to reproduce the production cross sections of mainly β-stable isotopes. This discrepancy may be however caused by another reaction mechanism, possibly a direct breakup in the field of heavy target nucleus, as suggested by the fact that production cross sections of these isotopes do not follow precisely the Q_{gg} systematics [38]. This assumption is supported also by the fact that discrepancies are observed mostly at lower angle and the effect increases with decreasing atomic number.

Collisions of ^{22}Ne+^{90}Zr at 7.9 AMeV

Projectile-like nuclei were observed also in the more symmetric reaction ^{22}Ne+^{90}Zr at beam energy 7.9 AMeV, using detector positioned at 12 deg [39]. The comparison of the observed isotopic yields (symbols) with the results of a standard PE+DIT/ICF+SMM simulation (dashed lines) and of the version using the DIT code with the extension of the nuclear profile (solid lines) is shown in Figure 26. The extension of the nuclear profile was again

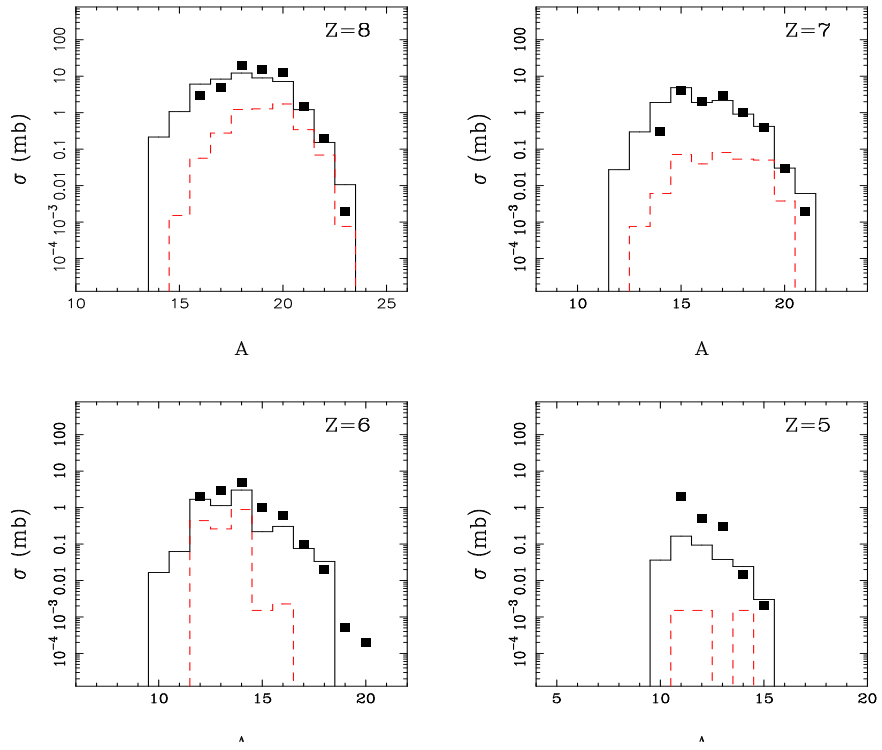

Figure 24: Experimental [38] (symbols) and simulated (lines) mass distributions in the reaction ^{22}Ne+^{232}Th at 7.9 AMeV for selected elements at 40 degrees. Dashed lines - standard PE+DIT/ICF+SMM simulation, solid lines - PE+DIT/ICF+SMM using the DIT code with the extension of the nuclear profile.

approximately 75 % compared to the three reactions at beam energy 5.5 – 6.0 AMeV. Again the standard PE+DIT/ICF+SMM simulation appears to underpredicts the magnitude of some observed cross sections, specifically for isotopes of oxygen and nitrogen. For these nuclei, improvement is achieved when using the extended nuclear profile, with the extension as in the reaction ^{22}Ne+^{232}Th. The evolution of the trend thus seems consistent with the dependence on the beam energy as in the previous cases, in this reaction, however, the effect is pronounced weakly when compared to the reactions with heavy fissile target nuclei, since the difference in the overall quality of agreement between two simulation is not too significant. It appears that the extension of nuclear profile evolves mostly in reactions where heavy fissile nuclei participate.

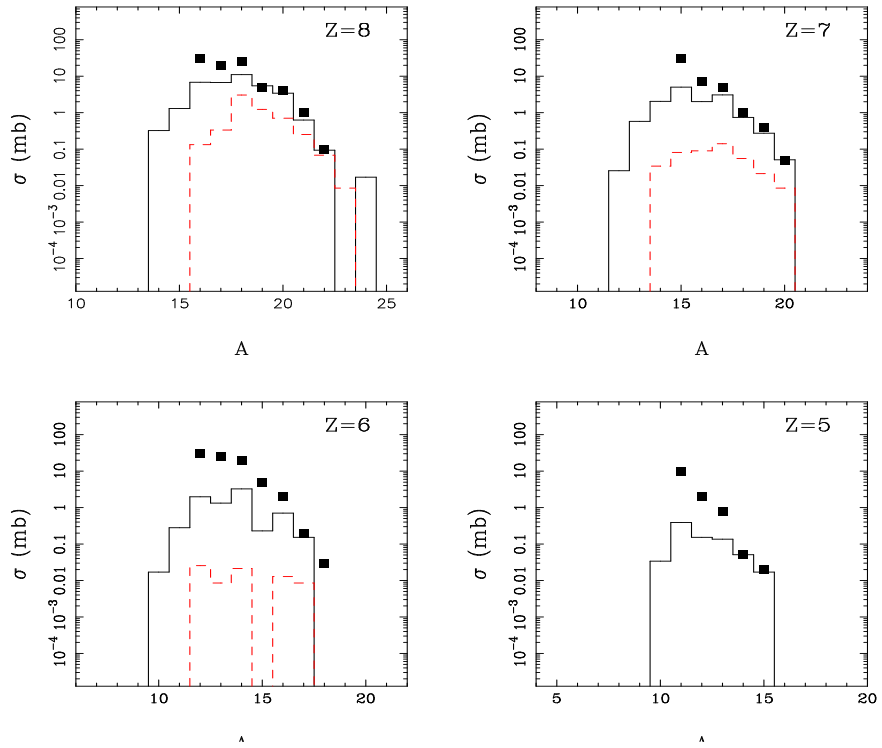

Figure 25: Experimental [38] (symbols) and simulated (lines) mass distributions in the reaction ^{22}Ne+^{232}Th at 7.9 AMeV for selected elements at 12 degrees. Dashed lines - standard PE+DIT/ICF+SMM simulation, solid lines - PE+DIT/ICF+SMM using the DIT code with the extension of the nuclear profile.

Experiment on production of neutron-rich nuclei around 15 AMeV

The reactions induced by beams with energy around 15 AMeV can in principle demonstrate both the reaction mechanisms known at energies close to the Coulomb barrier, such as the complete fusion, and reaction mechanisms, known at higher energies. The production cross sections at these energies are necessary in order to determine the optimum regime for production of exotic species, such as the optimum beam energy and target thickness. Until now, no high resolution heavy residue data existed in this region. In order to fill this gap, an experimental data at the beam energy 15 AMeV were obtained recently at the Cyclotron Institute of the Texas A&M University using the

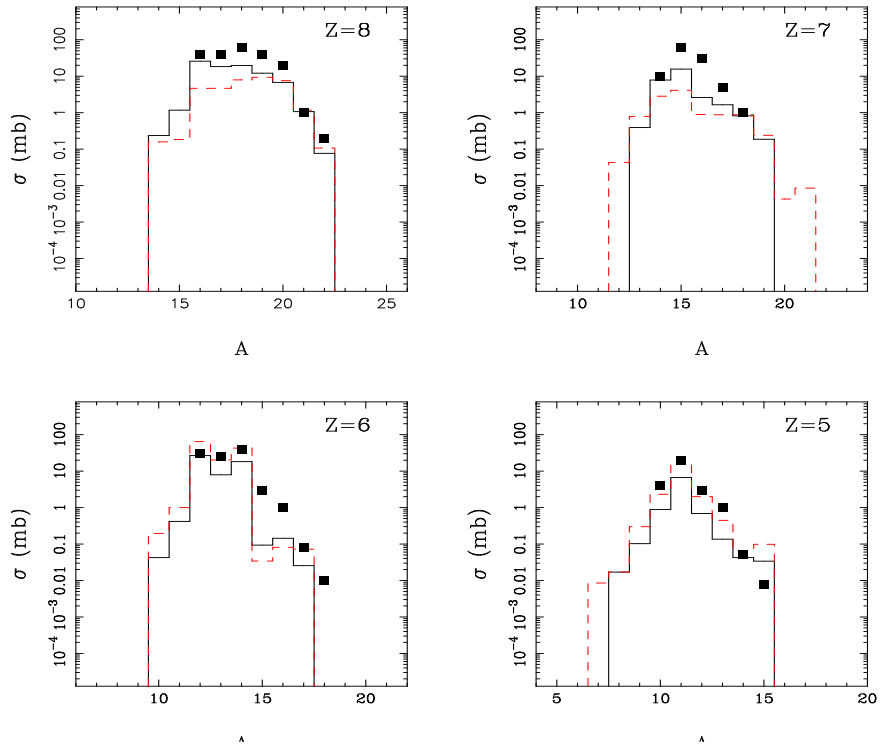

Figure 26: Experimental [38] (symbols) and simulated (lines) mass distributions in the reaction ^{22}Ne+^{90}Zr at 7.9 AMeV for selected elements at 12 degrees. Dashed lines - standard PE+DIT/ICF+SMM simulation, solid lines - PE+DIT/ICF+SMM using the DIT code with the extension of the nuclear profile.

recoil spectrometer MARS.

The study was performed at the Cyclotron Institute of Texas A&M University. A 15 AMeV ^{40}Ar and ^{86}Kr beams from the K500 superconducting cyclotron, with a typical current up to 10 pnA, interacted with ^{27}Al and ^{58,64}Ni targets of typical thickness around 2.0 mg/cm^2. The reaction products were analyzed with the MARS recoil separator [19]. The primary beam struck the target at 4 degrees relative to the optical axis of the spectrometer. The direct beam was collected in a small square Faraday cup. The fragments were accepted in the angular opening of MARS, in this setting in the range 2 - 6 degrees (angular acceptance of MARS is 9 msr). MARS optics provides one intermediate dispersive image and a final achromatic image (focal plane) and offers a momentum acceptance of 4%. At the focal plane, the

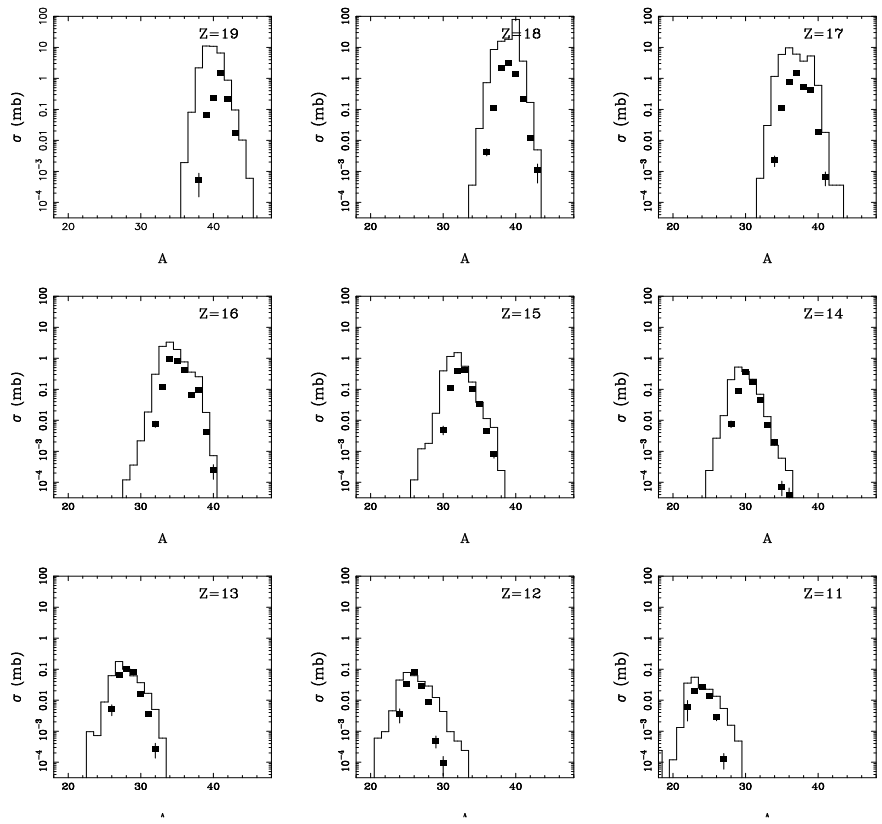

Figure 27: Mass yield curves from the reaction ^{40}Ar+^{27}Al at 15 AMeV at 4 degrees. Solid squares - measured data. Lines - result of the PE+DIT/ICF+SMM calculation [1, 4, 21] filtered by the spectrometer angular and azimuthal acceptance.

fragments were collected in a silicon detector telescope. The ΔE detector was a large area Si strip detector of 65 μm thickness, whereas the E detector was a single-element Si detector of 950 μm, respectively. Time of flight was measured between two parallel plate avalanche counters (PPACs) positioned at the dispersive image and at the focal plane, respectively, and separated by a distance of 13.2 m. The PPAC at the dispersive image was also X-Y position sensitive. The horizontal position, along with NMR measurements of the field of the MARS first dipole, was used to determine the magnetic rigidity Bρ of the particles. Thus, the reaction products were characterized by an event-by-event measurement of the energy loss, residual energy, time of flight, and magnetic rigidity. The response of the spectrometer and detector

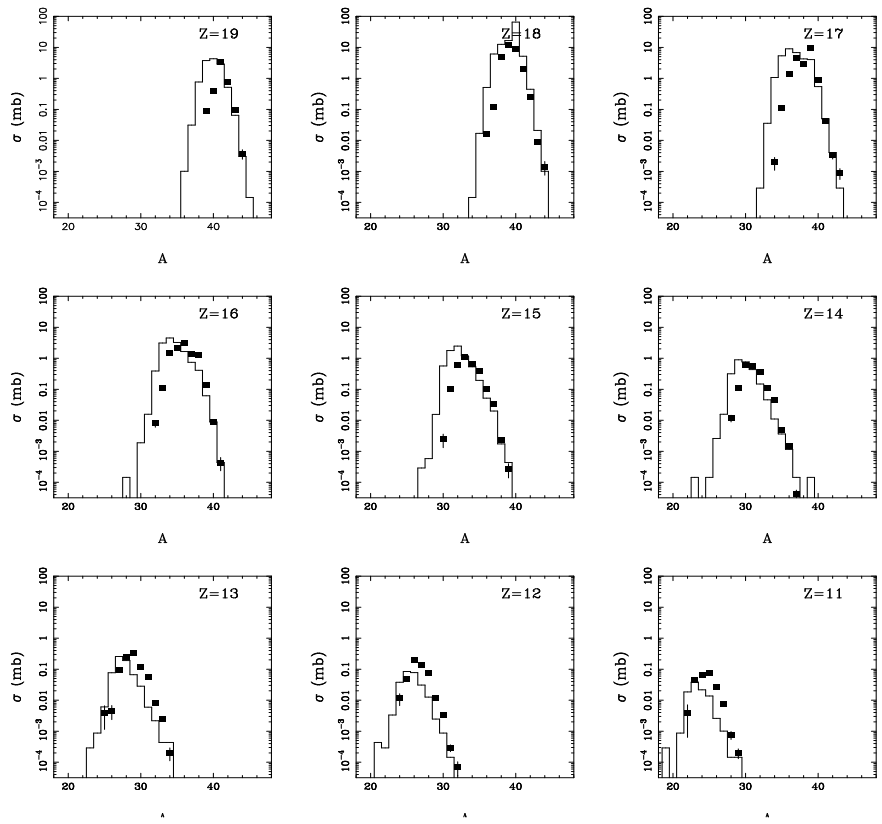

Figure 28: Mass yield curves from the reaction ^{40}Ar+^{64}Ni at 15 AMeV at 4 degrees. Solid squares - measured data. Lines - result of the PE+DIT/ICF+SMM calculation, filtered by the spectrometer angular and azimuthal acceptance.

system to ions of known atomic number Z, mass number A, ionic charge q and velocity was calibrated using low intensity primary beams. To cover the N/Z and velocity range of the fragments, a series of measurements were performed at overlapping magnetic rigidity settings in the range 1.1-1.5 Tesla-meters. The determination of the atomic number Z was based on the energy loss of the particles in the first ΔE detector and their velocity, with a resulting resolution (FWHM) of 0.6 Z units for A<90 . The ionic charge q of the particles entering the spectrometer after the Al stripper, was obtained from the total energy, the velocity and the magnetic rigidity. The measurement of the ionic charge q had a resolution of 0.5 Q units (FWHM) for A<90. Since the ionic charge must be an integer, integer values of q were assigned for each event by

putting appropriate windows on each peak of the q spectrum at each magnetic rigidity setting of the spectrometer. Using the magnetic rigidity and velocity measurement, the mass-to-charge A/q ratio of each ion was obtained and combining the q determination with the A/q measurement, the mass A was obtained. Combination and appropriate normalization of the data at various magnetic rigidity settings of the spectrometer provided fragment distributions with respect to Z, A, q and velocity. Correction of missing yields caused by charge changing at the PPAC (positioned at the dispersive image) was performed. The isotope distributions were subsequently summed over all values of q.

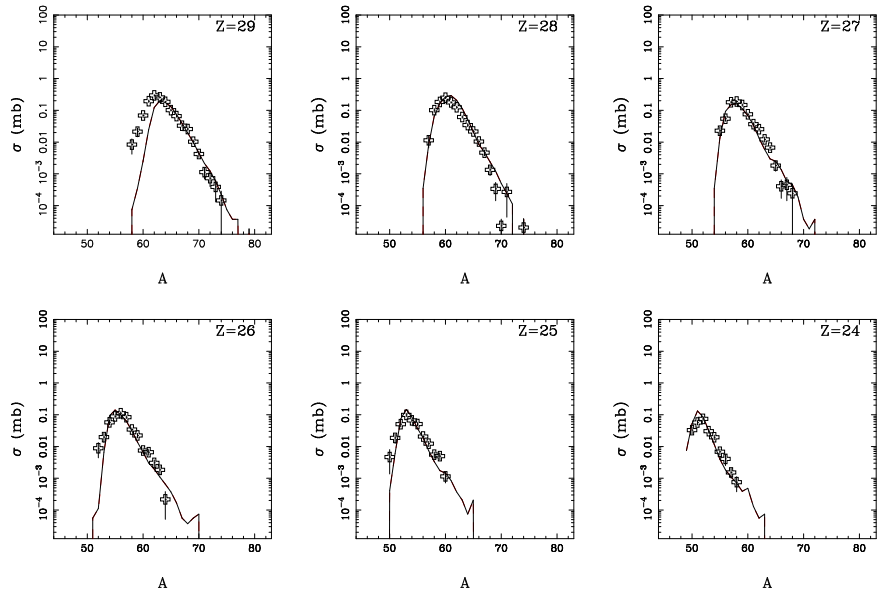

Figure 29: Mass yield curves from the reaction ^{86}Kr+^{64}Ni at 15 AMeV at 4 degrees. Symbols - measured data. Lines - result of the PE+DIT/ICF+SMM calculation, filtered by the spectrometer angular and azimuthal acceptance.

Figure 27 presents the mass yield curve from the reaction ^{40}Ar+^{27}Al at 15 AMeV at 4 degrees. The measured data, normalized for beam current and target thickness are presented as solid squares. The result of the PE+DIT/ICF+SMM calculation [1, 4, 21], filtered by the spectrometer angular and azimuthal acceptance is given by the full line. A comparison of the measured yields to the calculated filtered yields shows reasonable overall agreement for the projectile-like nuclei with Z=11-19. The discrepancies at

the proton-rich side can be caused by experimental (Bρ) limitations while for the three lightest elements similar limitations appear to be exhibited also on the neutron-rich side. In general one can consider that at 15 AMeV the PE+DIT/ICF+SMM simulation appears to be equally successful as at the energy 25 AMeV.

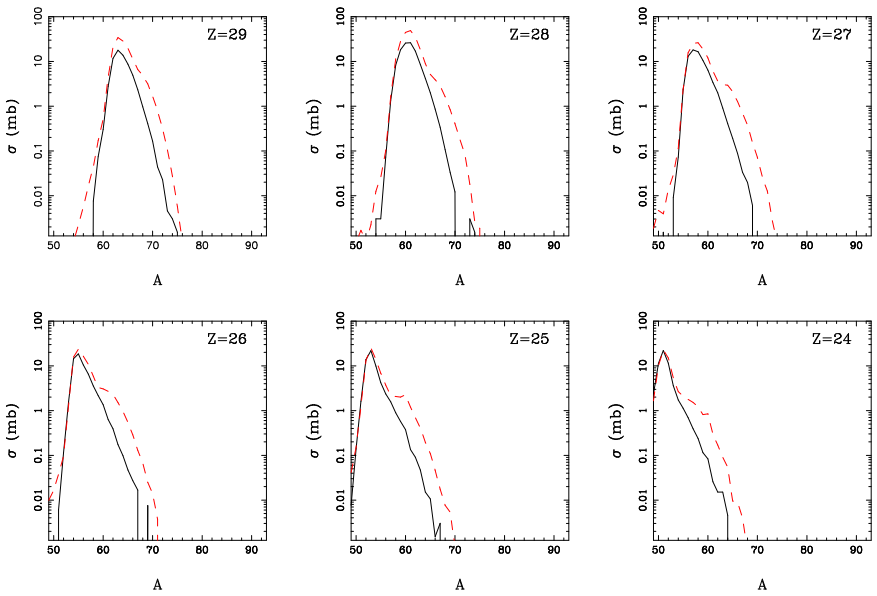

Figure 30: Calculated total mass yield curves from the reaction ^{86}Kr+^{64}Ni at 25 (solid lines) and 15 AMeV (dashed lines).

This conclusion is supported also by the mass yield curve from the reaction ^{40}Ar+^{64}Ni at 15 AMeV at 4 degrees shown in Figure 28. Also in this reaction the PE+DIT/ICF+SMM shows similarly successful as in the previous case. The apparent lack of the calculated yields for the three lightest elements can stem from more forward focused angular distributions of these products originating from ICF collisions, suggesting lower azimuthal factors than the average ones which were obtained assuming even spread of products over spectrometer coverage.

Figure 29 shows the results for the reaction ^{86}Kr+^{64}Ni at 15 AMeV, again at 4 degree setting. The products with Z=29-24 seem to be reproduced reasonably well.

Figure 30 shows the comparison of the calculated total isotopic yields

for the reaction ^{86}Kr+^{64}Ni at beam energies 15 and 25 AMeV. It can be seen that the production cross sections do not drop during transition from 25 to 15 AMeV, the shapes of mass distributions remain similar, with some possible excess of neutron-rich nuclei appearing at 15 AMeV, representing a component produced mostly at higher angles, which thus needs verification in corresponding measurement since the present measurement does not provide decisive answer.

Summary of the data analysis

Table 1 provides summary of the investigated reactions. The available data covers significant part of the matrix, with few exceptions at low and transitional energies. Table 2 provides overview of the dominant reaction mechanisms inside individual cells of the matrix. As one could expect, the scenario involving pre-equilibrium emission in the early stage followed by deep-inelastic transfer or incomplete fusion leads to consistent results in most of the cases above 10 AMeV. It nevertheless appears that participant-spectator scenario starts to play role at energies above 50 AMeV for very asymmetric projectile-target combinations. Also in this domain there are signals of the mechanism of neutron loss (dynamical emission) preceding the thermal equilibration of the massive projectile-like fragment. Such effect seems to be more pronounced in the case of proton-rich projectile-like fragments while in neutron-rich cases it may be overshadowed by intense statistical emission of neutrons. Signal of analogous behavior of neutron was observed also in the multifragmentation data in the work [5]. Also the behavior in semi-central collisions at lower energies [4], where fast transfer of multiple neutrons can be deduced, points toward non-standard dynamical evolution of neutrons, most probably in the neck region between the projectile and target. At the beam energies below 10 AMeV, deep-inelastic transfer appears to be dominant reaction mechanism, with the possible extended evolution of nuclear profile in the window (neck) region, mostly in the case of heavy target nuclei. It would be desirable to obtain experimental data at normal kinematics between 10-20 AMeV, where one can expect smooth transition between behavior at higher and lower energies, however it is interesting to determine maximum beam energy at which the low energy behavior

Table 1: Classification of investigated reactions based on mass asymmetry and beam energy

	Normal kinematics	Nearly symmetric	Inverse kinematics
Low energies up to 10 AMeV	^{58}Ni+^{208}Pb, E=5.7 AMeV [35] ^{64}Ni+^{208}Pb, E=5.5 AMeV [36] ^{64}Ni+^{238}U, E=6.1 AMeV [37] ^{22}Ne+^{232}Th, E=7.9 AMeV [38] ^{22}Ne+^{90}Zr, E=7.9 AMeV [39]		
Transitional energies from 10 to 20 AMeV		^{86}Kr+^{64}Ni, E=15 AMeV ^{40}Ar+^{64}Ni, E=15 AMeV ^{40}Ar+^{64}Ni, E=15 AMeV ^{124}Sn+^{124}Sn, E=20 AMeV [26]	^{124}Sn+^{27}Al, E=20 AMeV [18]
Fermi energy domain from 20 to 50 AMeV	^{129}Xe+^{197}Au, E=44 AMeV [27]	^{86}Kr+^{64}Ni, E=25 AMeV [2] ^{86}Kr+^{112,124}Ni, E=25 AMeV [3] ^{129}Xe+^{90}Zr, E=44 AMeV [27]	^{129}Xe+^{27}Al, E=26 AMeV [29] ^{129}Xe+^{27}Al, E=50 AMeV [29]
Fragmentation energies above 50 AMeV	^{86}Kr+^{181}Ta, E=64 AMeV [33]	^{78}Kr+^{58}Ni, E=75 AMeV [32]	^{86}Kr+^{27}Al, E=70 AMeV [31]

suggesting extended nuclear profile survives in the very asymmetric reactions with heavy target.

Estimation of production cross sections of exotic nuclei

Isoscaling as a tool for estimation of production cross sections of exotic nuclei

In the context of isotopic distributions, sensitivity to isospin degrees of freedom can be explored globally by investigating the ratio of isotopic yields from two processes with different isospin asymmetry, essentially dividing the two isotopic distributions in point-by-point fashion. When employing the statistical model, such a ratio will depend on N and Z as follows

$$R_{21}(N,Z) = Y_2(N,Z)/Y_1(N,Z) = C\exp(\alpha N + \beta Z) \tag{4}$$

where, in grand-canonical limit, $\alpha = \Delta\mu_n/\mathrm{T}$ and $\beta = \Delta\mu_p/\mathrm{T}$, $\Delta\mu_n$ and $\Delta\mu_p$ are the differences in the free neutron and proton chemical potentials of the fragmenting systems. C is an overall normalization constant. Alternatively the dependence can be expressed as

$$R_{21}(N,Z) = Y_2(N,Z)/Y_1(N,Z) = C\exp(\alpha' A + \beta'(N-Z)) \tag{5}$$

thus introducing the parameters which can be related to the isoscalar and isovector components of free nucleon chemical potential since $\alpha' = \Delta(\mu_n + \mu_p)/2\mathrm{T}$ and $\beta' = \Delta(\mu_n - \mu_p)/2\mathrm{T}$.

An exponential scaling of R_{21} with the isotope neutron and proton numbers was observed experimentally in the multifragmentation data from the reactions of high-energy light particles with massive target nucleus [40, 41] or from the reactions of mass symmetric projectile and target at intermediate energies [42] and such behavior is called isoscaling [42] (the parameters $\alpha, \beta, \alpha', \beta'$ being called isoscaling parameters). Isoscaling behavior was further reported in the heavy residue data [43] and also in fission data [44]. It

Table 2: Classification of principal reaction mechanisms based on mass asymmetry and beam energy

	Normal kinematics	Nearly symmetric	Inverse kinematics
Low energies up to 10 AMeV	Deep-inelastic transfer Extended nuclear profile ?		
Transitional energies from 10 to 20 AMeV		Pre-equilibrium emission Deep-inelastic transfer + Incomplete fusion	Pre-equilibrium emission Deep-inelastic transfer + Incomplete fusion
Fermi energy domain from 20 to 50 AMeV	Pre-equilibrium emission Deep-inelastic transfer + Incomplete fusion	Pre-equilibrium emission Deep-inelastic transfer + Incomplete fusion	Pre-equilibrium emission Deep-inelastic transfer + Incomplete fusion or Participant-Spectator Neutron loss ?
Fragmentation energies above 50 AMeV	Pre-equilibrium emission Deep-inelastic transfer + Incomplete fusion	Pre-equilibrium emission Deep-inelastic transfer + Incomplete fusion Neutron loss ?	Pre-equilibrium emission Deep-inelastic transfer + Incomplete fusion or Participant-Spectator Neutron loss ?

was shown that the values of isoscaling parameters can be related to symmetry energy [42, 41], to the level of isospin equilibration [43] and to the values of transport coefficients [44].

The isoscaling phenomena can be observed in the heavy residue data, collected at forward angles. Yield ratios $R_{21}(A, Z)$ of projectile residues from the reactions ^{86}Kr+^{124,112}Sn at 25 AMeV [45] were investigated and isoscaling behavior was observed for each isotopic and isotonic chain. The isoscaling slopes are constant for residue mass range A = 25 – 60, corresponding to primary events with the maximum observed excitation energy of 2.2 AMeV. The slopes exhibit gradual decrease with increasing mass of the residues. Assuming that the fragmentation occurs at normal density, using C_{sym} = 25 MeV [41], the values of isoscaling parameters can be used to determine the values of $\Delta(N/Z)_{qp}$ (where qp means quasi-projectile) as a function of the observed residue mass A and charge Z, thus demonstrating the evolution of the N/Z equilibration process in isospin-asymmetric collisions. The monotonic increase of $\Delta(N/Z)_{qp}$ with excitation energy can be understood as a result of the mechanism of nucleon exchange.

The Fig. 31 shows isoscaling plots in the reactions of ^{86}Kr (25AMeV) with ^{124,112}Sn. The simulation (curves) is the same as in [4] where it allowed to reproduce experimental cross sections for neutron-rich nuclides and residues from de-excitation of hot nuclei. Some discrepancies were observed in the yields of a limited set of β-stable nuclei close to the projectile, which were overestimated due to low probability for the emission of complex fragments below multifragmentation threshold. Experimental isoscaling plots are shown as symbols (starting from Z=34 solid squares, crosses, solid stars, open stars cyclically repeating). For nuclei with Z=25-30 the simulation and experiment lead to a similar behavior with constant slopes and consistent values of the isoscaling parameters. For heavier nuclei with N>44, the simulation leads to a reverse trend of the yield ratios toward unity, possibly signaling the onset of a reaction mechanism independent of the N/Z of the target, possibly quasi-elastic (direct) few-nucleon transfer taking place in very peripheral collisions. The experimental isoscaling behavior for these nuclei shows signs of a similar reverted trend, the transition is not as regular as in the simulation and the inclusion of the points from this region into the exponential fits (lines) leads to a decrease of the apparent isoscaling slopes. Such decrease of the slope of exponential ("isoscaling") fits is shown by the straight lines despite the very poor quality of such fits. Thus the evolution of the apparent exponential slopes in both experimental and simulated data

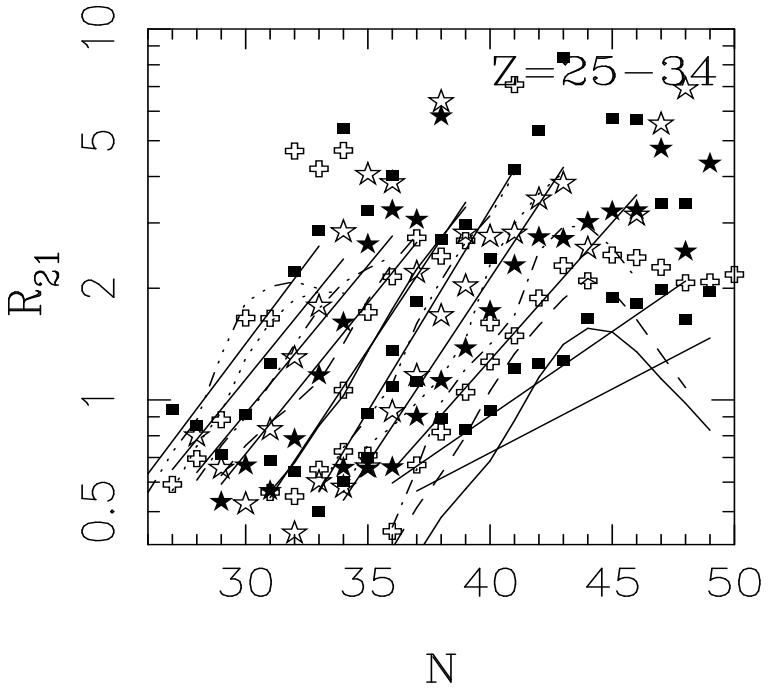

Figure 31: Isoscaling plot for the reactions of ^{86}Kr+^{124,112}Sn at incident energy of 25 AMeV. Curves - simulated data for fragments with Z=25-34, symbols - experimental data [3]. The straight lines represent exponential fits of the simulated data.

suggest a mixing of two components: one component very sensitive to the N/Z of the target, possibly due to an intense nucleon exchange; a second component, insensitive to the N/Z of the target, possibly quasi-elastic few-nucleon exchange. It is apparent that in the region with regular isoscaling behavior one can attempt to extrapolate the trend to more exotic species.

The Fig. 32 shows isoscaling plots in the reactions of ^{40}Ar (15AMeV) with ^{64,58}Ni. Meaning of lines and symbols is identical to previous figure. Experimental data, presented in the previous section, ehxibit isoscaling behavior, which in this case is reproduced by the simulation, with some discrepancy around and above of N=20 shell closure. Even if the effect of shell structure is seen both in the experiment and simulation, simulation (specifically the SMM de-excitation code) appears to overestimate it.

The Fig. 33 shows isoscaling plots in the reactions of ^{64,58}Ni with ^{208}Pb at beam energies close to 5.5 AMeV (see previous section). Meaning of lines

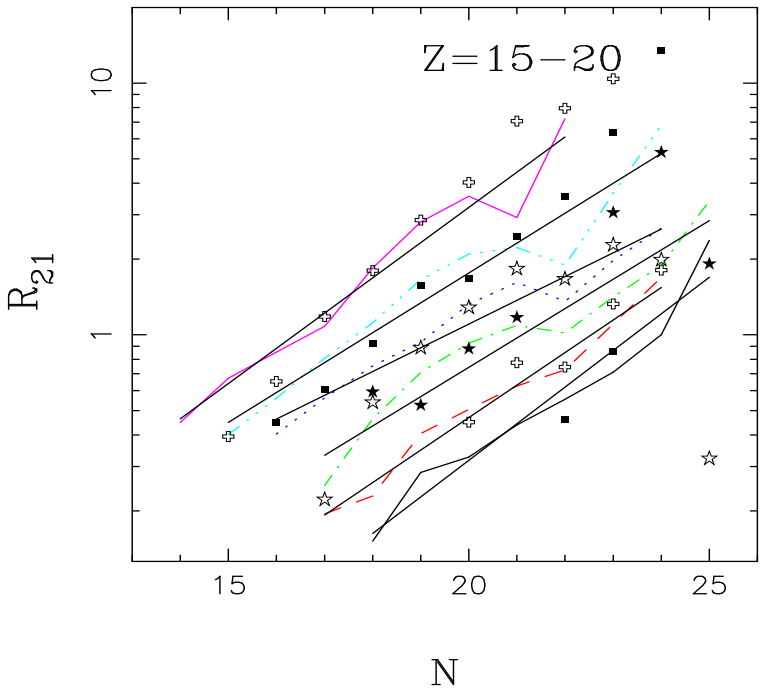

Figure 32: Isoscaling plot for the reactions of ^{40}Ar+^{64,58}Ni at incident energy of 15 AMeV. Curves - simulated data for fragments with Z=15-20, symbols - experimental data. The straight lines represent exponential fits of the simulated data.

and symbols is identical to previous figure, starting from Z=27 and down, isoscaling plots are shifted up by order of magnitude for each charge unit. It is remarkable that isoscaling behavior is preserved even at low energies close to the Coulomb barriers and such observation supports the conclusion that deep-inelastic transfer is the main contributing mechanism even at such low energies, despite some addiotional features due to evolution of the mean field. Furthermore, unlike the previous plots, in this case the isoscaling is observed in the case of two reactions where different beams hit the same target. Observation of isoscaling in this case shows that isoscaling can be in principle used for prediction of production rates in the reactions of exotic secondary beams. If the reaction mechanism is well understood and one can assume that the behavior will persist even for exotic beams, one can extrapolate the evolution of the isoscaling slopes, proportionally to the shift in the neutron number (of other measure of isospin asymmetry), and predict, using

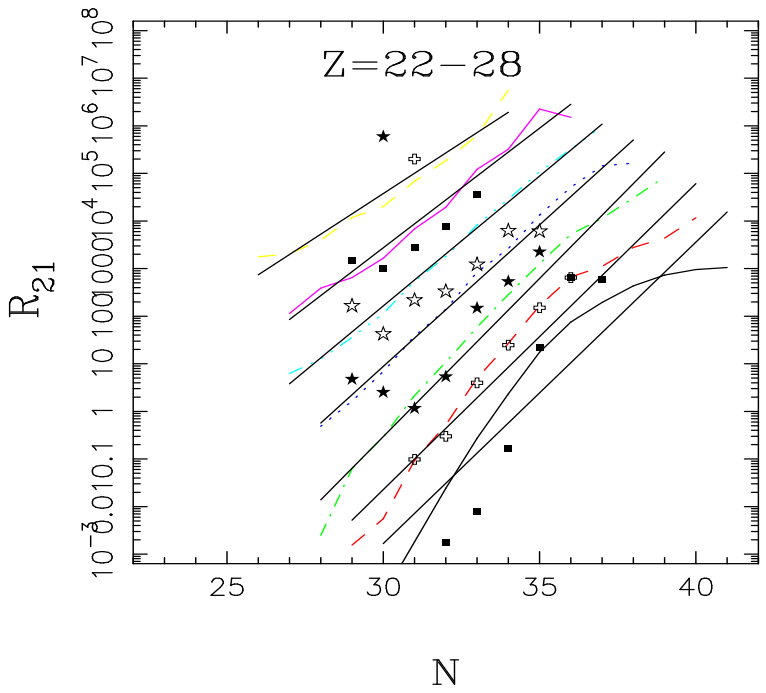

Figure 33: Isoscaling plot for the reactions of ^{64,58}Ni+^{208}Pb at incident energy around 5.5 AMeV. Curves - simulated data for fragments with Z=22-28, symbols - experimental data. The straight lines represent exponential fits of the simulated data. Starting from Z=27 and down, isoscaling plots are shifted up by order of magnitude for each charge unit.

the yields measured with less exotic or stable beams, the production cross sections of very exotic species. Such a method can be a welcome tool for experimentalists. Nevertheless, additional work is still needed, specifically to carry out pairs of experiments with different beams under identical conditions. This method is natural for the deep-inelastic collisions, which appear to cover the energy range from the Coulomb barrier up to even 60-70 AMeV (see previous section), one can in principle to consider its application even for fragmentation reactions, where however, as demonstrated e.g. in the theoretical works [46, 47, 48], regular isoscaling behavior can be expected mostly far from the projectile, while close to the projectile the behavior reflects the lack of isospin equilibration due to nucleon exchange with the light target.

Estimation of production cross sections of nuclei around ^{78}Ni

As a part of the EU 6FP project EURISOL Design Study, a comparison of various mechanisms, representing possible scenarios of the primary linear accelerator, was carried out in terms of production of the exotic nuclei [49]. Production cross section estimates for nuclear reactions around the Fermi energy were shown to be competitive in comparison to estimates for fragmentation reactions, in particular for very neutron-rich products. The use of intense heavy ion beams at the EURISOL's primary accelerator was not considered in the final design due to limited technical and financial resources.

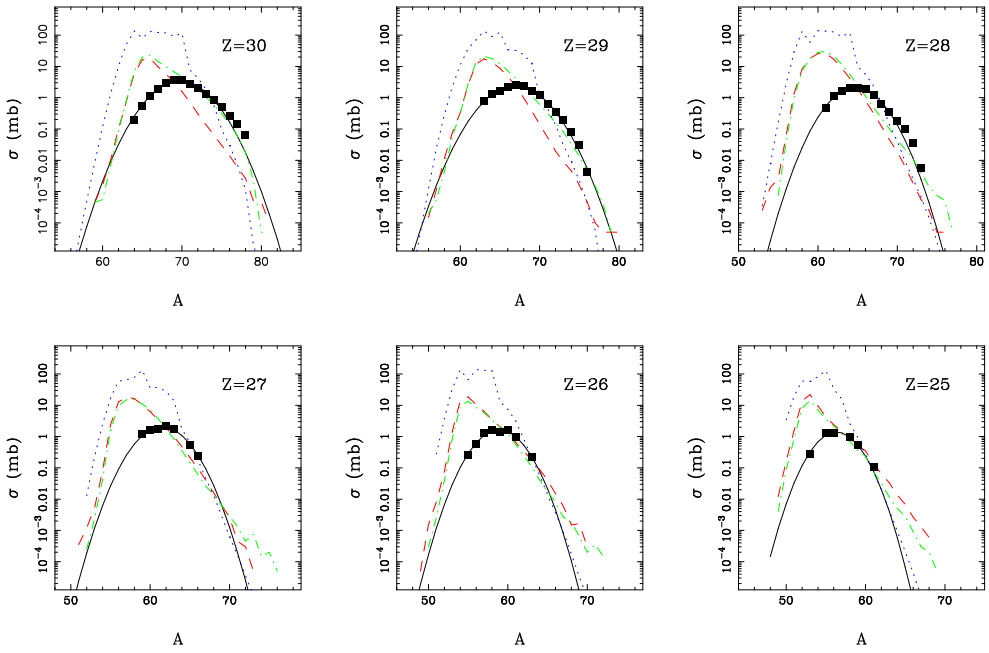

Figure 34: Production cross sections of isotopes of Zr and elements below. Symbols - experimental data for reaction of 1 GeV protons with ^{238}U [50], solid lines - Gaussian fits of experimental mass distributions, dotted lines - estimates of production cross sections in fragmentation of stable nuclei, obtained using EPAX [20] by optimization for each nucleus separately, dashed and dash-dotted lines - production cross sections for reactions of ^{86}Kr,^{82}Se+^{64}Ni at 25 AMeV, calculated using the PE+DIT/ICF+SMM simulation.

Figure 34 shows a comparison of the production of element Zr and below. The experimental spallation cross sections for the reaction of 1 GeV protons with ^{238}U [50] is represented by symbols and solid lines, representing Gaussian fits of the experimental mass distributions. The estimates of production cross sections in fragmentation of stable nuclei, obtained using EPAX [20] by optimization for each nucleus separately are represented by dotted lines.

The production cross sections for the reactions of ^{86}Kr,^{82}Se+^{64}Ni at 25 A MeV, were calculated using the PE+DIT/ICF+SMM framewrok [4] (dashed and dash-dotted lines), described in the previous sections. One can see that the estimated optimum fragmentation cross sections essentially follow the experimental trend as described by the Gaussian fits. On the other hand, the production cross sections in the reactions of ^{86}Kr,^{82}Se+^{64}Ni at 25 MeV appear to dramatically overshoot the experimental trend for spallation of ^{238}U, thus indicating that this option can be competitive even despite its limitations on target thickness. In order to explore such excess in cross sections, heavy ion beams of high intensities must be available and new experimental techniques for extraction and formation of secondary beams need to be developed.

Production of neutron-rich nuclei around N=82

One of the promising ways to produce extremely neutron-rich nuclei around the neutron shell N=82 is fragmentation of a secondary beam of ^{132}Sn. Nevertheless, based on the results of the previous sections, one can in principle consider also the reaction in the Fermi-energy domain at energies below 50 AMeV. The comparison of production cross sections for the reaction ^{132}Sn+^{238}U at 28 AMeV with fragmentation cross section of ^{132}Sn beam with Be target is provided in Fig. 35. For the reaction ^{132}Sn+^{238}U the PE+DIT/ICF+SMM simulation was used, while for the fragmentation of ^{132}Sn beam the codes COFRA [51] (dotted lines) and EPAX [20] (dash-dotted lines) were used. The production cross sections calculated using both the original and modified model of incomplete fusion for Z=46 are comparable with results of EPAX and COFRA, while for elements with lower atomic numbers the reaction ^{132}Sn+^{238}U leads, to increasingly favorable cross sections exceeding both COFRA and even EPAX cross sections.

The in-target yields calculated using the production cross sections obtained using PE+DIT/ICF+SMM and Cofra are shown in Fig. 36. For the fragmentation of ^{132}Sn secondary beam an energy 100 AMeV was used, the value foreseen for Eurisol [52]. The achievable in-target reaction rate was

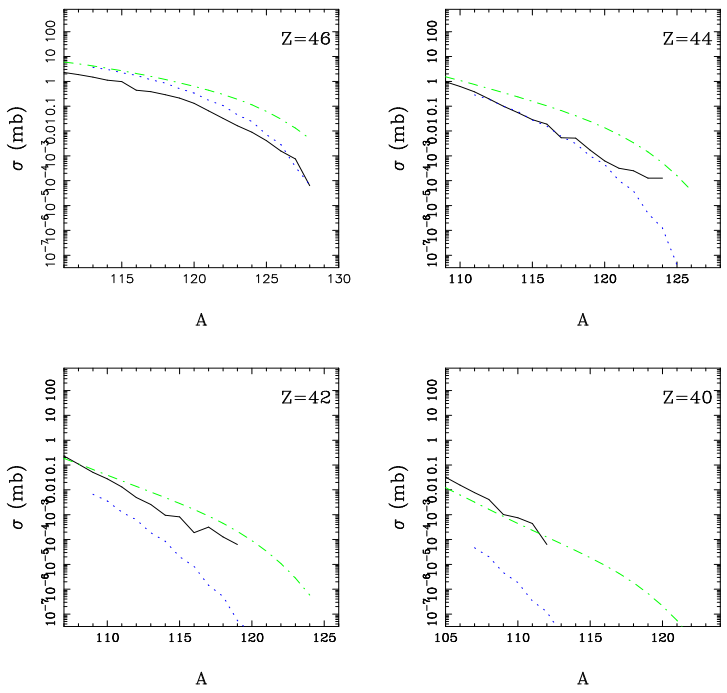

Figure 35: Comparison of production cross sections for reaction ^{132}Sn+^{238}U at 28 AMeV using PE+DIT/ICF+SMM simulation (solid lines) with fragmentation cross sections of ^{132}Sn beam with Be target using COFRA [51] (dotted lines) and EPAX [20] (dash-dotted lines).

determined using code AMADEUS [53]. For the reaction ^{132}Sn+^{238}U at 28 AMeV a target thickness 40 mg/cm^2 was assumed. For the intensity of ^{132}Sn secondary beam a value of 10^{12} s^{-1} was adopted from Eurisol RTD Report [52]. Due to larger target thickness, the in-target yield for fragmentation option calculated using COFRA dominate for elements Z=44 and above, for lighter nuclei nevertheless the larger production cross sections in the Fermi-energy domain lead also to larger in-target yields despite relatively thin target and for Z=40 such in-target yields exceed the COFRA value. The COFRA values were used for fragmentation since several recent measurements show that EPAX overpredicts the yields of neutron-rich nuclei. For instance, fragmentation experiment with ^{86}Kr beam carried out at MSU [54] showed that experimental fragmentation cross section of neutron-rich Ni isotopes are overpredicted by EPAX by up to two orders of magnitude. The recent experiment

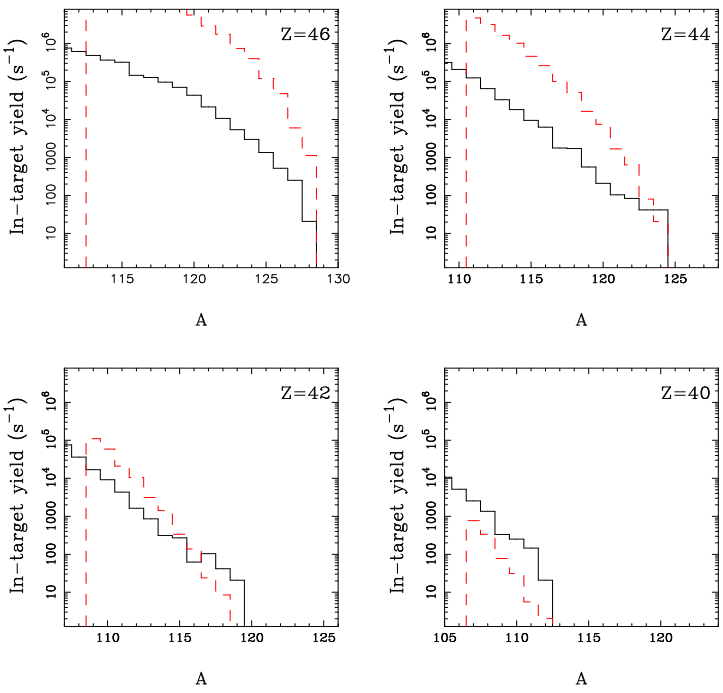

Figure 36: The in-target yields (for the intensity of ^{132}Sn beam 10^{12} s^{-1}) calculated using the production cross sections from Fig. 35. Solid lines - ^{132}Sn+^{238}U at 28 AMeV, PE+DIT/ICF+SMM simulation, dashed lines - fragmentation of 100 AMeV ^{132}Sn beam with Be target using COFRA [51].

on the fragmentation of ^{132}Sn beam, performed within the Task 11 of Eurisol Design Study, demonstrated that predicitions of Cofra are favorable for neutron-rich nuclei. Thus it appears that the reactions in the Fermi-energy domain can become interesting. However, the angular distribution of reaction products below 50 AMeV would require a large-acceptance separator with angular coverage up to 10 degrees, wide charge state acceptance and a highly efficient gas-cell in order to form a secondary beam.

Technical aspects of secondary beams in the Fermi energy domain

The analysis presented in the previous sections allows to assume the reactions in the Fermi energy domain as a possible source of neutron-rich nuclei for secondary beam formation. A logical continuation of the present study is the investigation of the practical aspects and specifically the possibilities to produce reaction products with optimum mixture and properties for subsequent formation of the secondary beams using the ISOL (IGISOL) method. The kinetic energy of the products will limit the possible target thickness and, due to the wide angular and charge distributions, the in-flight method for the formation of secondary beams would not lead to high quality beams. As relatively suitable appears the possibility to use a version of the ISOL method, where the products will be stopped in the gas volume (gas cell) and subsequently extracted, charge-bred and formed into a beam. Such a solution is in principle verified and practically used to form secondary beams of the fission products or products of fragmentation reactions [55, 56].

One additional goal of further development is to explore a solution for the optimum target setup and subsequent separation and modification of the properties of the reaction products for further use as secondary beams. It will be necessary to use the production cross sections of the very netron-rich nuclei in reactions at beam energies around the Fermi energy, depending on the beam energy and emission angle, as an input for the target simulation, specifically for the optimization of the yields of desired products while preserving the properties allowing their susbsequent separation from other products, most notably particles of the scattered beam.

For the subsequent separation we can assume a system consisting of a large-bore superconducting solenoid (of typical magnetic field of 5-7 Tesla) along the lines described in [57]. The primary beam will be collected with an on-axis blocker covering the angular range 0 to 2 degrees. The deep inelastic products, along with the elastically scattered beam will pass the solenoid and will be focused into a gas cell after traversing appropriate diagnostic detectors (e.g. PPAC, ionization chamber etc.) and a degrader of appropriate thickness. After that point, the techniques developed in [55, 56] can be applied to extract and form the RIB. In order to increase the flexibility and separation ability of such a system, the option of employing two solenoid magnets will be explored in detail. With a dual solenoid system, additional

purification of the RIB mixture can be achieved with appropriate diaphragms and/or degrader at the intermediate focus, in addition to the possibility of obtaining a good TOF measurement between a PPAC at this location and the PPAC at the final focus. Depending on the reaction of choice, the angular range up to 10 degrees should be adequate to collect the products of interest from heavy-ion reactions in the Fermi energy regime.

Along with studies of separator configuration, it is necessary to continue the experimental measurements of cross sections and study of their dependence on isospin asymmetry. To carry out such measurements it is necessary to have available intense beams of nuclei such as isotopic pairs ^{40,48}Ca, ^{58,64}Ni, ^{78,86}Kr, ^{112,124}Sn, ^{124,136}Xe with energy at least 20 - 30 AMeV and intensity at least 1 pnA, ideally more. Pairs of isobaric or isotonic beams can be also considered, since isoscaling can be defined in regards to the dependence on isospin.

Summary and conclusions

The available experimental data from nucleus-nucleus collisions at beam energies from the Coulomb barrier up to 70 AMeV and various projectile-target asymmetries were investigated. The scenario involving pre-equilibrium emission in the early stage followed by deep-inelastic transfer or incomplete fusion leads to consistent agreement in most of the cases. It nevertheless appears that the participant-spectator scenario starts to play role at energies around 50 AMeV for very asymmetric projectile-target combinations in inverse kinematics. At beam energies around and above 50 AMeV there are signals of the mechanism of neutron loss (dynamical emission) preceding the thermal equilibration of the massive projectile-like fragment. Such effect seems to be clearly pronounced in the case of proton-rich projectile-like fragments while in neutron-rich cases it may be overshadowed by intense statistical emission of neutrons. Signal of analogous behavior of neutrons was observed also in the multifragmentation data [5]. Also at beam energies below 10 AMeV, deep-inelastic transfer appears to be the dominant reaction mechanism, with contribution from the possible extended evolution of nuclear profile in the window (neck) region, mostly in the case of heavy target nuclei.

In general the achieved level of understanding of the reaction mechanism provides a suitable starting point to consider production of secondary beams in the Fermi energy domain. The comparison with other reaction do-

mains, such as spallation and fragmentation, suggests that this option can be competitive for production of very neutron-rich nuclei around the N=50 and N=82 shell closures. Observation of isoscaling, namely the exponential scaling of product yields with initial isospin of the projectile-target system, can in principle be used for prediction of production rates in the reactions of exotic secondary beams. If the reaction mechanism is well understood, assuming that the behavior will persist even for exotic beams, one can extrapolate the evolution of the isoscaling slopes, proportionally to the shift of isospin asymmetry, and predict, using the yields measured with less exotic (or stable) beams, the production cross sections of very exotic species.

Production of secondary beams in the Fermi energy domain requires specific technical solutions, including ion-optical devices with angular acceptance up to 10 degrees, such as superconducting solenoids, and effective event-by-event tagging procedure for an in-flight scenario or a highly effective gass cell for production of high-purity secondary beams. A comparative advantage is offered by the possibility that the primary beam can be easily eliminated, since the majority of exotic products is emitted at angles away from zero degrees.

References

[1] M. Veselsky, Nucl. Phys. A 705 (2002) 193.

[2] G.A. Souliotis et al., Phys. Lett. B 543 (2002) 163.

[3] G.A. Souliotis et al., Phys. Rev. Lett. 91 (2003) 022701.

[4] M. Veselsky, G.A. Souliotis, Nucl. Phys. A781 (2007) 521.

[5] M. Veselsky et al., arXiv:0801.3140 [nucl-ex].

[6] M. Veselsky et al., Effect of nucleon exchange on projectile multifragmentation in the reactions of Si-28+Sn-112 and Sn-124 at 30 and 50 MeV/nucleon - art. no. 064613, PHYSICAL REVIEW C 2000, Vol 6206, Iss 6, pp 4613-+

[7] L. Tassan-Got, PhD Thesis, 1988, Orsay, France, IPNO-T-89-02, 1989; Deep-inelastic transfer: A way to dissipate energy and angular momentum for reactions in the Fermi energy domain, L. Tassan-Got, C. Stefan, Nucl. Phys. A 524 (1991) 121

[8] J.P. Bondorf et al., Phys. Rep. 257 (1995) 133.

[9] Systematics of complex fragment emission in niobium-induced reactions, R. Charity et al., Nucl. Phys. A 483 (1988) 371

[10] N. Matsuoka, A. Shimizu, K. Hosono, T. Saito, M. Kondo, H. Sakaguchi, Y. Toba, A. Goto, F. Ohtani, N. Nakanishi, Nucl. Phys. A **311** (1978) 173.

[11] J. Gosset, H.H. Gutbrod, W.G. Meyer, A.M. Poskanzer, A. Sandoval, R. Stock, G.D. Westfall, Phys. Rev. C **16** (1977) 629.

[12] A.Y. Abul-Magd, Z. Phys. A **298** (1980) 143.

[13] B.G. Harvey, M.J. Murphy, Phys. Lett. B **130** (1983) 373.

[14] J.-J. Gaimard, K.-H. Schmidt, Nucl. Phys. **A 531** (1991) 709.

[15] J. Randrup, R. Vandenbosch, Nucl. Phys. A **474** (1987) 219.

[16] W. Hauser, H. Feshbach, Phys. Rev. 1952. V.87. P.366.

[17] L.G. Moretto, Nucl. Phys. A. 1975. V.247. P.211.

[18] M. Veselsky et al., Heavy-residues with A¡90 from the asymmetric reaction of 20 A MeV 124Sn + 27Al as a sensitive probe of the onset of multifragmentation, Nucl. Phys. A 724 (2003) 431.

[19] R.E. Tribble, R.H. Burch and C.A. Gagliardi, Nucl. Instr. and Meth. A285 (1989) 441; R.E. Tribble, C.A. Gagliardi and W. Liu, Nucl. Instr. and Meth. B56/57 (1991) 956.

[20] K. Summerer, B. Blank, Phys. Rev. C 61 (2000) 34607.

[21] M. Veselsky, G.A. Souliotis, Nucl. Phys. A 765 (2006) 252.

[22] G. Audi and A.H. Wapstra, Nucl. Phys. A 565 (1993) 1.

[23] W.D. Myers and W.J. Swiatecki, Nucl. Phys. A 81 (1966) 1.

[24] G. Casini et al., Phys. Rev. Lett. 71 (1993) 2567; C.P. Montoya et al., Phys. Rev. Lett. 73 (1994) 3070.

[25] U. Brosa et al., Phys. Rep. 197 (1990) 167.

[26] G.A. Souliotis et al., Production and separation of neutron-rich rare isotopes around and below the Fermi energy, Nucl. Instr. Meth. B 204 (2003) 166.

[27] J. Feng et al., Phys. Rev. C 50 (1994) 2420.

[28] L. Bianchi et al., Nucl. Instr. and Meth. A 276 (1989) 509.

[29] K.A. Hanold et al., Phys. Rev. C 52 (1995) 1462.

[30] B.M. Sherill et al., Nucl. Instr. and Meth. B56/57 (1991) 1106.

[31] R. Pfaff et al., Phys. Rev. C 51 (1995) 1348.

[32] R. Pfaff et al., Phys. Rev. C 53 (1996) 1753.

[33] M. Mocko et al., arXiv:0705.4313 [nucl-ex]

[34] T. Kubo et al., Nucl. Instr. and Meth. B70 (1992) 309.

[35] L. Corradi et al., Nucl. Phys. A 701 (2002) 109c.

[36] W. Krolas et al., Nucl. Phys. A 724 (2003) 289.

[37] L. Corradi et al., Nucl. Phys. A 734 (2004) 237.

[38] A.G. Artukh et al., Nucl. Phys. A 283 (1977) 350.

[39] V.V. Volkov, Phys. Rep. 44 (1978) 93.

[40] O.V. Lozhkin, W. Trautmann, Phys. Rev. C. 1992. V.46. P.1996.

[41] A.S. Botvina et al., Phys. Rev. C. 2002. V.65. P.44610.

[42] M.B. Tsang et al., Phys. Rev. Lett. 2001. V.86. P.5023.

[43] G.A. Souliotis et al., Phys. Rev. C. 2003. V.68. P.24605.

[44] M. Veselsky, G.A. Souliotis, M. Jandel, Phys. Rev. C. 2004. V.69. P.44607.

[45] G.A. Souliotis et al., Phys. Lett. B. 2004. V.588. P.35.

[46] C.W.Ma, Y.Fu, D.Q.Fang, Y.G.Ma, X.Z.Cai, W.D.Tian, K.Wang, C.Zhong, Int. J. Mod. Phys. E17, 1669 (2008);

[47] D.Q.Fang, Y.G.Ma, C.Zhong, C.W.Ma, X.Z.Cai, J.G.Chen, W.Guo, Q.M.Su, W.D.Tian, K.Wang, T.Z.Yan, W.Q.Shen, J.Phys.(London) G34, 2173 (2007)

[48] C. Zhong, Y. G. Ma, D. Q. Fang, X. Z. Cai, J. G. Chen, W. Q. Shen, W. D. Tian, K. Wang, Y. B. Wei, J. H. Chen, W. Guo, C. W. Ma, G. L. Ma, Q. M. Su, T. Z. Yan, J. X. Zuo, Chin. Phys. 15 (2006) 1481-1485.

[49] SCHMIDT, Karl-Heinz, KELIC, Aleksandra, LUKIC, Strahinja, RICCIARDI, Maria-Valentina, VESELSKY, Martin; Benefits of extended capabilities of the driver accelerator for EURISOL, Physical Review Special Topics Accelelerators and Beams 10, 014701 (2007)

[50] M. Bernas et al., Nucl. Phys. A 725 (2003) 213

[51] K. Helariutta, J. Benlliure, M. V. Ricciardi, K.-H. Schmidt, Eur. Phys. J A 17 (2003) 181.

[52] EURISOL Feasibility Study RTD,
$http://www.ganil.fr/eurisol/Final\_Report.html$

[53] $http://www-w2k.gsi.de/charms/amadeus.htm$

[54] A. Stolz et al., Nucl. Phys. A 746 (2004) 54c.

[55] G. Savard et al., Nucl. Instr. Meth. B 204 (2003) 582.

[56] G. Bollen et al., Nucl. Instr. Meth. A 550 (2005) 27.

[57] G.A. Souliotis et al., Nucl. Instr. Meth. B 266 (2008) 4692.